HERA Memo 31: The new HERA 75Ω receiver

Nima Razavi-Ghods, Steve Carey, John Ely, Tian Huang

July 2017

Abstract

In this memo we describe the design of the new 75Ω receiver system for HERA. The design includes front-end matching and low noise considerations as well as interface and housing. Various measurement results including receiver temperature and simulated scan sensitivity are presented. This memo will be accompanied by an assembly manual which describes the process of assembly in the field.

In order to design the new front-end system, the existing design was examined and many of its useful features were retained, whilst others were improved. Based on the work carried out, the performance of the telescope should be improved with respect to sensitivity and match performance (i.e. spectral response of the antenna). Furthermore, the system bandwidth will be extended by 40MHz allowing good performance across 90-210 MHz and there will be improved intermodulation and compression performance to allow operation at the increasing RFI levels on site. The work carried out in this phase will help guide the next design phase which will incorporate the new antenna feeds.

Contents

1 Introduction

A new 75Ω receiver system has been developed for the HERA instrument. It consists of two principle components, known as the front-end module (FEM) and the post-amp module (PAM). The FEM-75 and PAM-75 units have been developed to work over the existing HERA band of 100-200 MHz, however they have adequate performance over the extended band of 50-210 MHz. In fact they should extend the system bandwidth from 110-190 MHz to 90-210MHz where the current feeds still provide decent performance.

The final HERA receiver system will be adapted to a new feed and will also work at 50Ω not to mention it will likely rely on RF-over-Fibre (RFoF) technology as the primary mode of signal transport and will incorporate various features like phase switching and noise calibration. That system is intended for Q3 2018, where it is envisaged that a total of 240 antennas will be deployed [1]. Prior to that deployment, a 75Ω "replacement" system has been developed to operate via the existing 150 meter RG-6 cables and therefore fitting the current interfaces and housing requirements.

There are several important reasons for developing such a system prior to the 240 roll-out. The chief reason being that much of the front-end circuitry, namely the Low Noise Amplifier (LNA) and matching circuit may remain the same or have a similar topology. Therefore, this allows the low-noise capabilities of the new system to be tested. Furthermore, questions regarding interface, housing, grounding and ESD/TVS protection, marking/barcodes/datalogging, and deployment can be tested using this 75Ω system because many of these features will be the same in the final design.

In the following sections, we describe the FEM and PAM designs and their measurement results including receiver temperature and intermodulation performance. A final table showing the performance summary will be provided in the last section.

2 Front-end module overview

2.1 Low noise amplifier and matching

The Front-end module is the most important RF component in the chain and it should be designed with careful attention on the matching to the antenna. There are essentially two aspects of the matching for the HERA front-end and these are noise matching and power matching. In radio astronomy applications, one of the most important criteria is to find an LNA which has an optimal noise impedance (by analysing the noise circles) that is close to the antenna impedance, thus ensuring that the best noise match is achieved and in turn this will reduce the receiver temperature and increase sensitivity. However, this is not the primary criteria for HERA, where roll off of the antenna (delay) spectrum is equally, if not more critical. The figure of merit which has been described in various papers including [1] is that the internal reflections should be attenuated by approximately 60 dB from the initial incoming wave by around 60 ns.

Unfortunately for most systems, these two aspects of the matching are a trade-off and both cannot be optimised together. This therefore made the FEM design more complex since the objective was to achieve the best of both worlds. It will be useful in the next design phase to perform some further analysis on this tradeoff.

In order to aid with this trade-off, a simple differential matching circuit was designed. It should be noted that any matching circuit will tend to increase the noise figure since it will have some loss, therefore it was determined that a good starting point would be a three section circuit which could have some impact on the power match whilst not degrading the noise performance. The reason for this being differential and not single-ended was that the LNA topology implemented for the FEMs was designed to feed each dipole arm to an LNA and combine the outputs with a balun in order to form a single ended output. This is often referred to as a Pseudo-differential configuration and one which results in very low noise since placing a balun prior to the LNA will dramatically affect the noise performance due to the balun's insertion loss which even in the best cases is of order 0.5dB (35K) for chip baluns. Another low noise configuration is one where the antenna has an integrated feeding structure allowing a single ended output, however this is only applicable for certain types of antennas.

By examining the reflection coefficient (S11) of the antenna when placed on the dish (approximately 5m above the base hub), it is possible to understand the matching requirement. Figure 1 shows the measured S-parameters of the antenna at the HERA site in South Africa (SA) and at Lord's Bridge (LB) located in Cambridge. The measurements in SA are significantly more noisy due to poor calibration of the VNA. These measurements are made with a straight through module and combined to form the differential S11. Although balun measurements were also made, the direct (straight through) measurements are seen as more accurate since the balun does not need careful de-embedding. The difference between the two plots is a shift in frequency and an increase in the reflection. This has since been described as being due the different heights of the feeds. The LB dish feed was at a height of 4.9m, whilst the SA feed was at a height of 5.16m. It is understood the SA feeds are now being lowered to be more reflective of the Cambridge dishes, therefore for the analysis in this memo we have used the LB data.

The S11 measurements were made with a balun and straight through module shown in Figure 2. This 2:1 chip balun used is based on model ADT2-1T-1P+ from minicircuits and was chosen not because it had the lowest loss but because it has an excellent amplitude and phase unbalance spec in the HERA band. For this reason, it is also the balun used in the FEM after the first stage LNA.

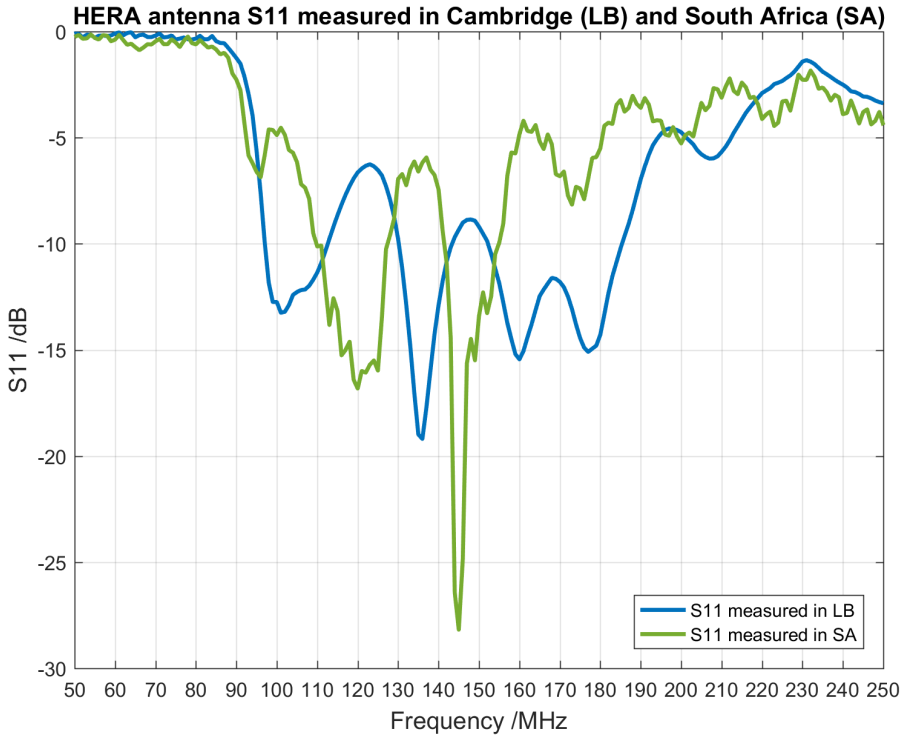

Figure 1: S11 measurements of HERA dish feed at two sites.

To find the best noise match, a range of LNAs were examined including but not limited to Minicircuits PGA-103+, SAV-551+, PSA4-5043+, and Triquint TQL9066, TQP3M903, the latter two being dual chip package LNAs. From early analysis and noise parameter measurements carried out by a PNA-X, we determined that Minicircuits PGA-103+ offered the best compromise. It was not the best in terms of noise performance and was not provided as a dual package, yet it could be better matched to the antenna.

In order to reduce the impact of receiver temperature, T_{rec}, standard noise parameters are used

$$F = F_{min} + \frac{4R_n}{Z_0}\left(\frac{|\Gamma_{opt} - \Gamma_{ant}|^2}{|1+\Gamma_{opt}|^2(1-|\Gamma_{ant}|^2)}\right) \tag{1}$$

where F_{min}, R_n, Γ_{opt}, and Γ_{ant} are the minimum noise factor, the equivalent noise resistance, the optimum noise reflection coefficient of the LNA and the reflection coefficient of the antenna, respectively.

One of the difficulties in choosing LNAs in this frequency band is that noise parameters are not provided by the manufacturers, who tend to focus on digital TV and cellular frequencies, therefore it is almost impossible to find properly measured noise parameters in the 50-200 MHz band. Instead there are two ways of working around this, either extrapolating down to low frequencies which is not always accurate due to the variation of noise parameters as a function of frequency or by direct measurements using a noise tuner which is effectively used to measure points on the smith chart and determine the optimal noise impedance. This too is rather difficult as low frequency noise tuners are very expensive and cumbersome to use. Our Keysight PNA-X provided an internal tuner which was used to measure these parameters, albeit with a limited number of measurement points around the smith chart.

In order to carry out the matching exercise, Keysight Genesys RF simulation package was used alongside Modelithics which provided accurate substrate scalable models of various inductors and capacitors. The design was then optimised within Genesys for VSWR/Mismatch loss (MLdB) and noise figure (NF). Whilst the exact roll-off the antenna spectrum could be simulated in EM simulation packages such as CST, matching between the antenna and front-end is achieved simply by aiming to reduce VSWR or mismatch loss which have the following relationship

$$MLdB = -10\log_{10}\left\{1-\Gamma^2\right\} \tag{2}$$

where

$$\Gamma = \frac{VSWR-1}{VSWR+1} \tag{3}$$

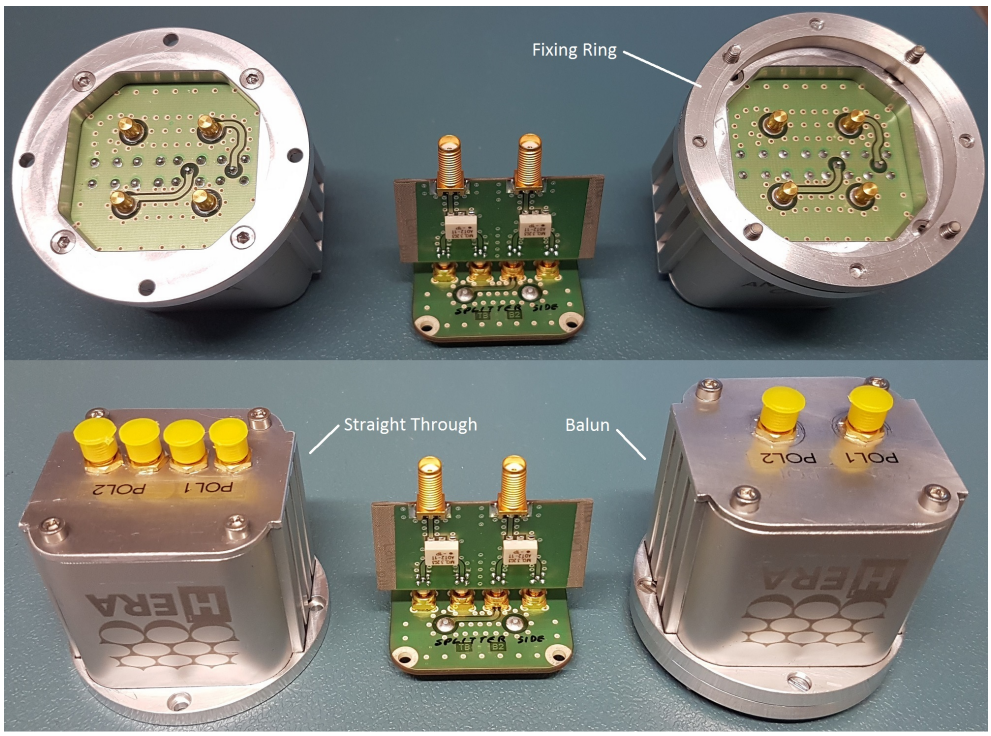

Figure 2: HERA RF balun and straight-through module.

Using the design frequency of 110-190MHz, our modest design goal was for NF less than 1.2dB (92K), VSWR less than 3.3 (or mismatch loss less than 1.5dB) allowing the ripple of the transducer gain (antenna + LNA gain) to be within ± 1dB.

The final active matching network is shown in Figure 3 with the simulated NF and transducer gain in Figure 4 taking into account the impedance of the antenna. The simulation here also included the second stage LNA which is described in the next section. Figure 5 shows the simulated mismatch loss (MLdB) for different matching extremes. Here we include the optimal NF option where the criteria is NF less than 1dB (75K) and the optimal power match design where NF is less than 1.6dB (129K). The final trade-off design is close to the match design whilst not degrading noise performance. Comparisons between the measured MLdB of the new and original receiver designs are shown later.

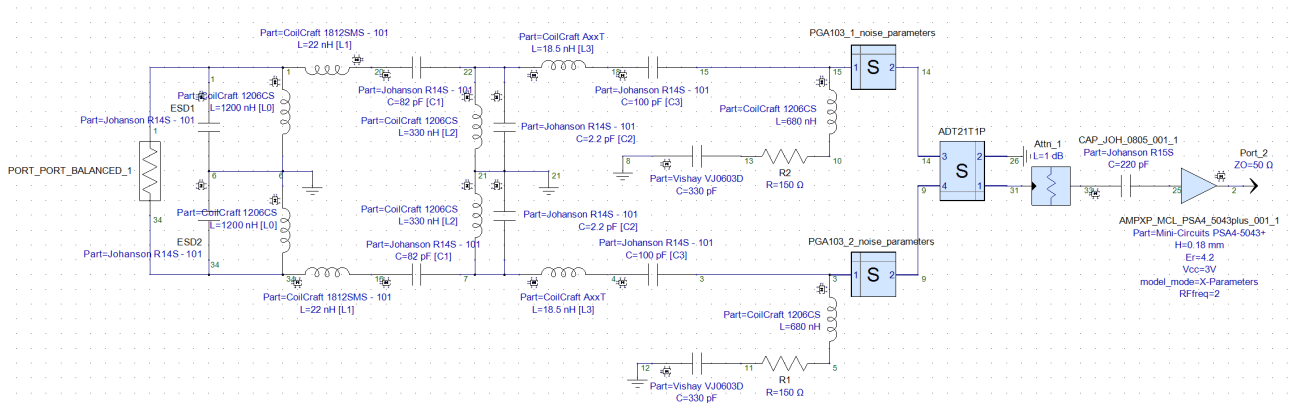

Figure 3: FEM active matching circuit.

For the PGA-103+ amplifier, the stability factor, K, was marginally lower than 1 between 50-100 MHz and therefore an LCR network was added to ensure the LNA was unconditionally stable at all frequencies. The resistor in this LCR network increases the NF slightly, however it is a small price to ensure stability across the whole band.

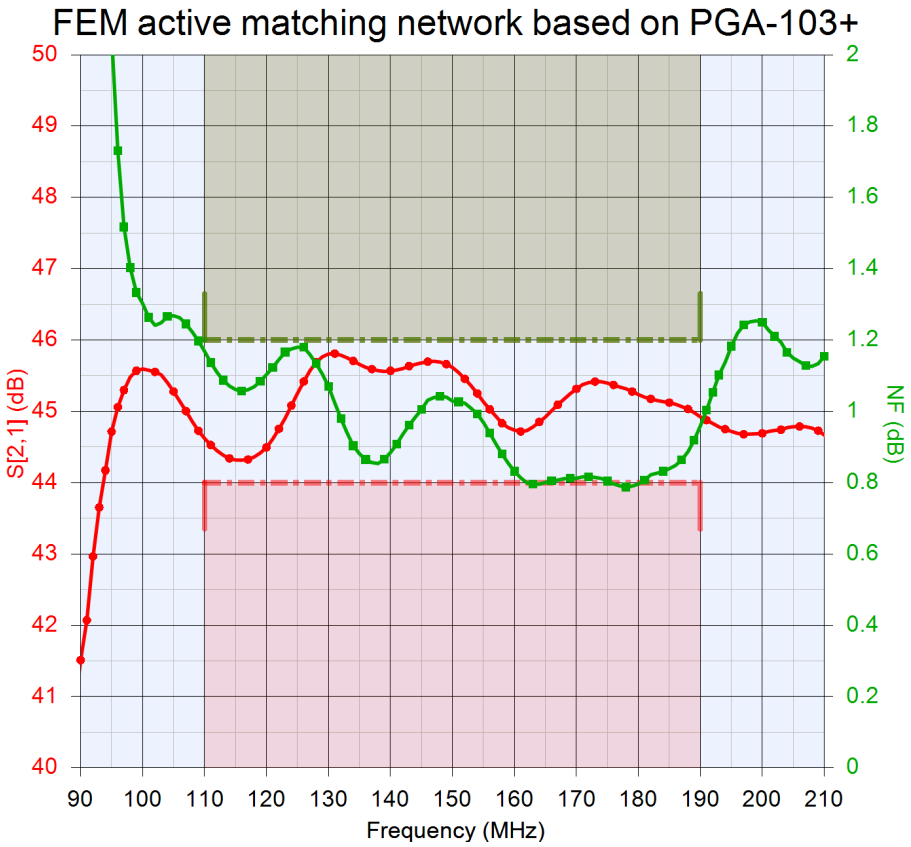

Figure 4: FEM active matching circuit transducer gain (S21) and NF.

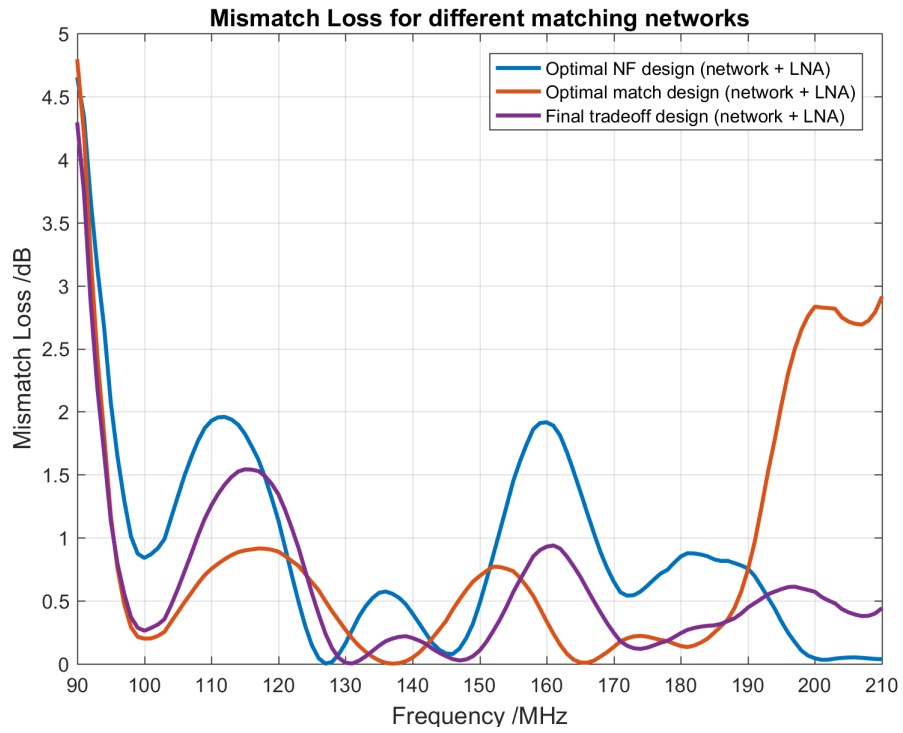

Figure 5: Mismatch loss of different active matching circuits.

2.2 Circuit design

All the designs presented here have been simulated using Keysight Genesys and some elements in MATLAB. After simulating the performance of the RF system, measuring prototype circuits such as LNAs and examining choke devices, we settled on the schematic for the FEM shown in Figure 6.

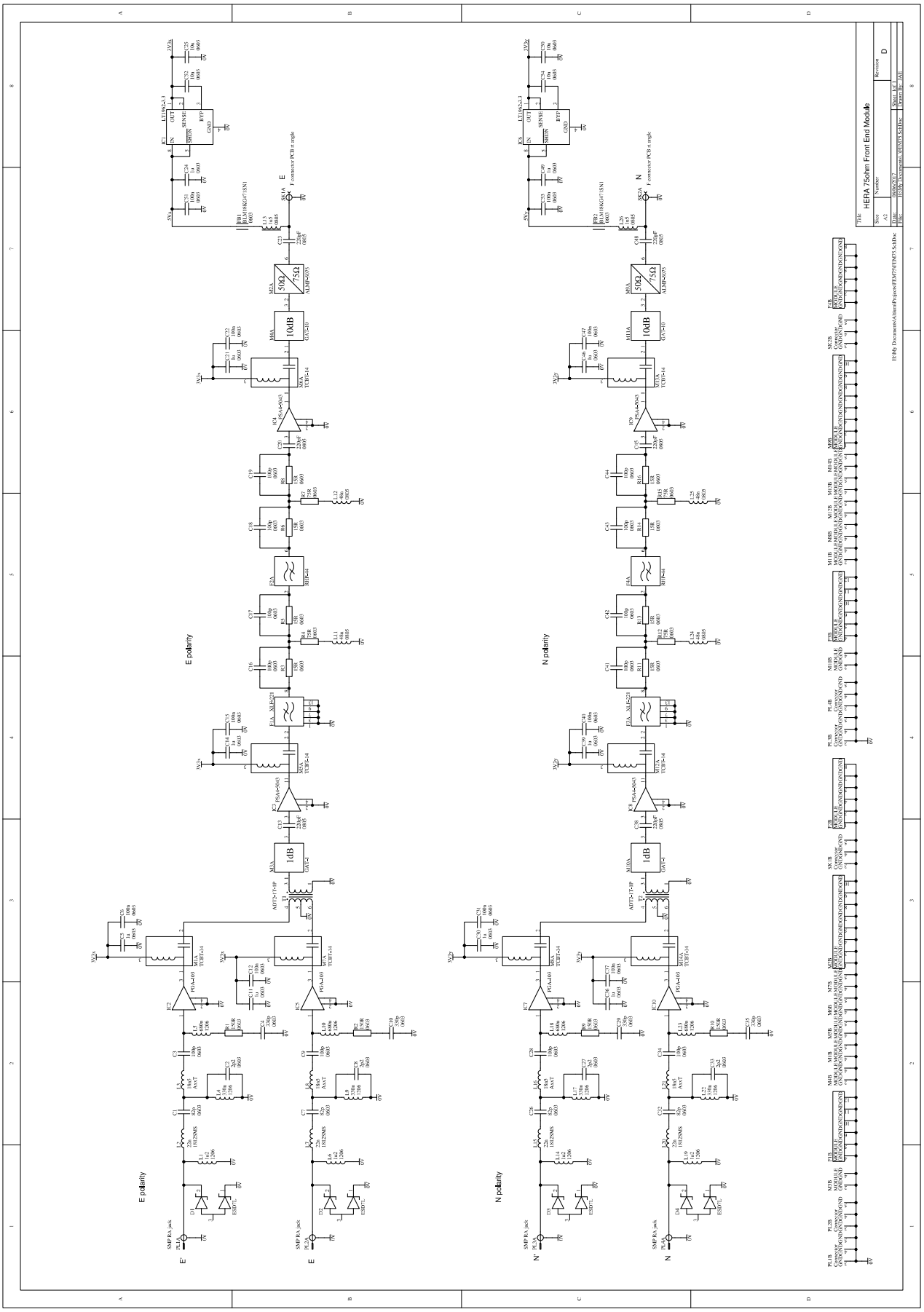

Figure 6: Front-end module schematic (E and N polarisation).

Before the active matching network, transient voltage suppression (TVS) is achieved by protection diodes ESD7L5.0DT5G. These diodes have a capacitance of 0.25pF and as such are represented by a capacitor in Figure 3. The FEM RF chain, then has 3 amplification stages, these are the first LNA (PGA-103+) followed by two more LNAs (PSA4-5043+). The latter component serves as all the gain blocks in the RF chain including in the PAM. It was chosen not because it is low noise, but due to the excellent intermodulation performance. As described by the Friis noise formula, the NF of the subsequent stage has minimal impact on the receiver temperature (or NF) of the system due to the fact that their noise contribution is divided down by the gain of the preceding stages. All the gain stages have some form of attenuation (padding) to help improve match performance.

For filtering, the FEM has a slow roll-off reflectionless low-pass filter (XLF-221+). This just ensures high frequency RFI (outside the HERA band) does not enter the chain. A custom made 9 section low pass filter in the PAM does the sharp filtering. A high pass filter (RHP-44+) filters anything below 44 MHz and was chosen so the FEM-75 could be used by other feed prototypes, especially the wideband feeds covering the band 50-210 MHz.

At multiple stages a T-section equalisation circuit was used to achieve a +2dB/100MHz slope across the band. This was to account primarily for the negative slope caused by the 150m RG6 cables as well as the amplification blocks in the chain. The total system gain is approximately 80dB including the loss of the long cable, with approximately 46dB of that being proportioned to the FEM. The total slope across the HERA band is less than 2dB.

The design of the FEM/PAM are essentially 50Ω and only converted to 75Ω at the cable end. This is achieved by a resistive impedance transform. Both circuits also incorporate a 10dB pad prior to this impedance transform in order to reduce the reflections back and forth on the long cables.

The FEM circuit is "phantom powered" through the F-type output connectors so the RF and DC are running on the coaxial cable. The advantage of this is that it is a clean shielded way of supplying the power without additional wires/cables being needed and breaks with the existing method of powering via the extra conductor in the cables. Each polarisation is fed separately via a low profile choke (0805AF-152XJRB), and the DC is then regulated by a low dropout regulator (LDO). All the amplifiers including the LNAs are fed by their own minicircuits choke (TCBT-14+).

Each polarisation draws approximately 200mA, and the cables have a DC resistance of 12Ω ±1Ω, therefore we would on average expect a voltage drop across the cable of 2.4V and this could be as high as 3V when taking into account the different cable lengths and temperature variations. Therefore as described in the next section, the PAMs provide a DC power output of 8V to ensure the LDOs on the PCB turn on and regulate. Everything on the FEM operates at 3.3V and the LT1962 LDO chosen for this circuit has a wide input voltage range up to 20V and is rated at 300mA, not to mention is has a very low noise level of 20μVrms. The recommended input voltage is 3.7V, which would allow some headroom when powering these devices in the field.

2.3 PCB and housing

A new interface and housing has also been developed for the FEM circuit. The existing PAPER sleeve dipole antenna as described in [2] outputs each dipole arm onto a Winchester Electronics PowerSnap (40A) receptacle connector. These power connectors can provide a good connection for RF. The 4 receptacle connectors reside on the antenna mating board which is part of the antenna assembly and this is where we define the interface from the antenna to the front-end electronics. The FEM is designed to connect to this mating board similar to the previous design. However, unlike the previous design, there is a transition from the horizontally mounted snap on connectors to a row of RF connectors so that a standard PCB could be used to connect to the antenna. This transition from horizontal to vertical is done with the "transition board" shown in Figure 7.

The PowerSnap connectors used on the transition board were designed and manufactured in house for more precise PCB positioning as compared to the original Winchester model. As for the RF connectors, SMP was the chosen snap-on connector due to its excellent axial and radial misalignment specifications. The FEM boards would then snap in to the transition board jacks which have "Catcher's Mitts" for easy alignment. SMP barrels connect the transition board and FEM connectors.

The FEM PCB layout was made as a 4-layer design with the stack-up being Signal-ground-ground-signal. The substrate used was FR4 with dielectric constant, ϵ_r of 4.2 and a height of 0.11mm on the top and bottom layers. The PCB's were made with a significant ground track between the two polarisation's to reduce cross-talk with the aim being approximately -50 to -60dB. The final assembled PCB is shown in Figure 8.

The housing developed for the FEM-75 was primarily based on a low-cost COTS extruded aluminium body (Fischer Elektronik GP222), available in 1m lengths. This was cut to 162mm in length for each FEM, allowing 6 per unit length. On the antenna side, a flange was designed to fit this housing with a laser cut rubber gasket for weather proofing. At the other end where the F-type connectors are located, an aluminium bottom plate would seal the box. To fit the FEM to the antenna mating board, an adaptor ring would need to be attached to the lower disc of the antenna. The primary purpose of this ring is to allow a 45 degree rotation of the module.

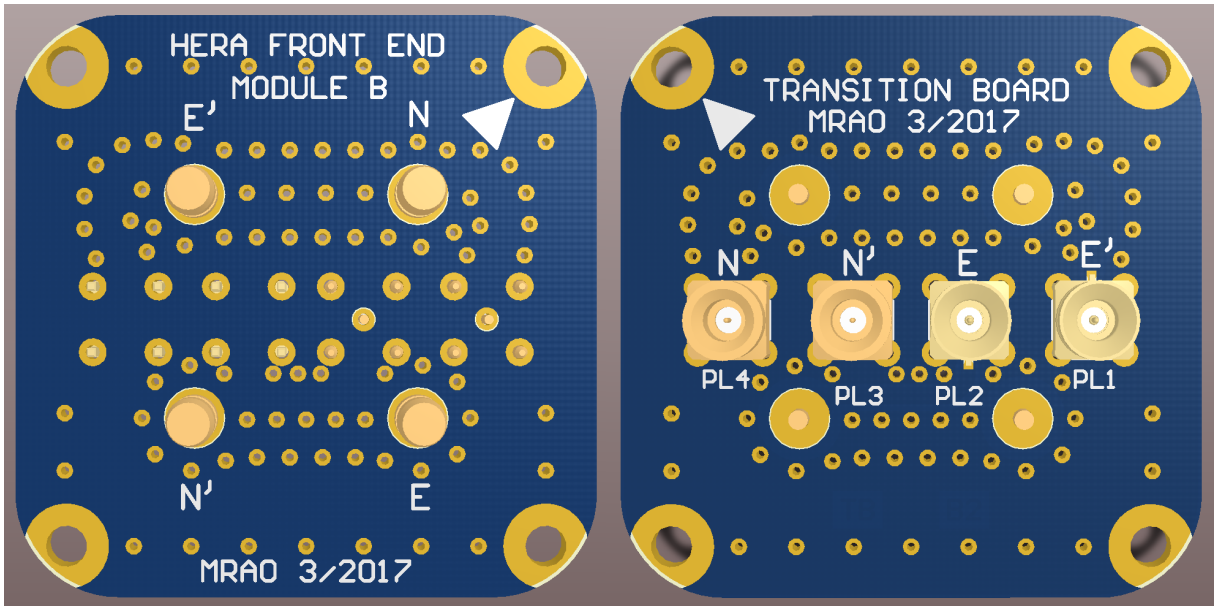

Figure 7: Front-end module transition board front and back.

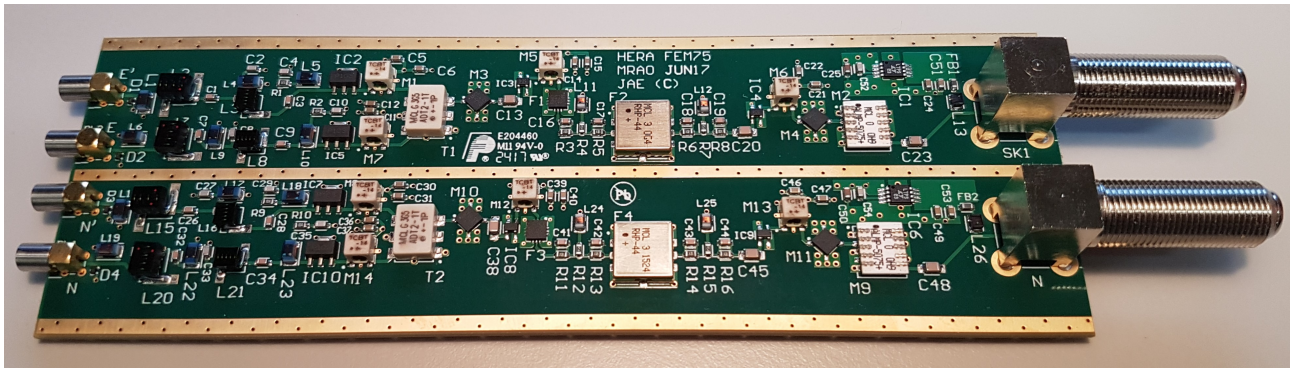

Figure 8: Front-end module PCB.

For the previous design, the entire FEM circuitry could be rotated 360 degree, however in the new design the orientation of the boards and the square body mean that the adapter ring is needed to ensure the module fits onto the antenna in the correct way. The assembly document [3], describes this in more detail as well as giving a glossary of the different components. Figure 9 shows the final FEM-75 inside the casing and Figure 10 shows its assembly onto the lower disc of the antenna.

The FEM housing components, namely the main body, flange, bottom plate and the adaptor ring were Alacrom plated, which is a conductive anodising that provides excellent corrosion protection. Each long edge of the FEM boards were then covered in a conductive tape (Laird Technology type 1A0254R) to ensure a good galvanic connection to the body when inside. The main body was also powder coated white to reduce heating of the modules in the Karoo.

In order to avoid confusion in the field, the same screws are used to attach the adapter ring to the lower disc and then the FEM onto the adaptor ring. These are UNC 4-40 x 1/4 inch screws requiring a 3/32" (2.38mm) hex key. Each module has a "North" marker and the two polarisations, labelled E and N are stamped on the bottom plate. Each module is given a unique barcode and a general QR code which points to the hera.mrao.cam.ac.uk site. Here all the data relating to the modules is made available. This is described in more detail in the following sections.

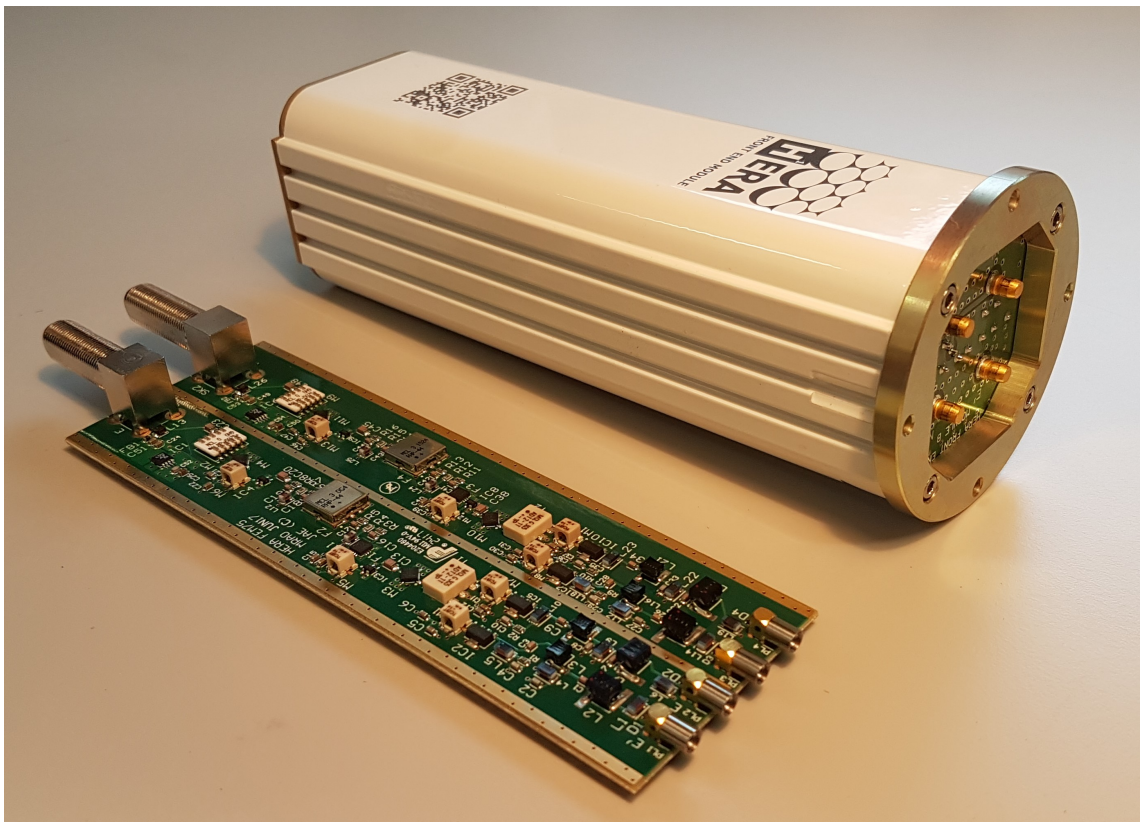

Figure 9: Front-end module housing.

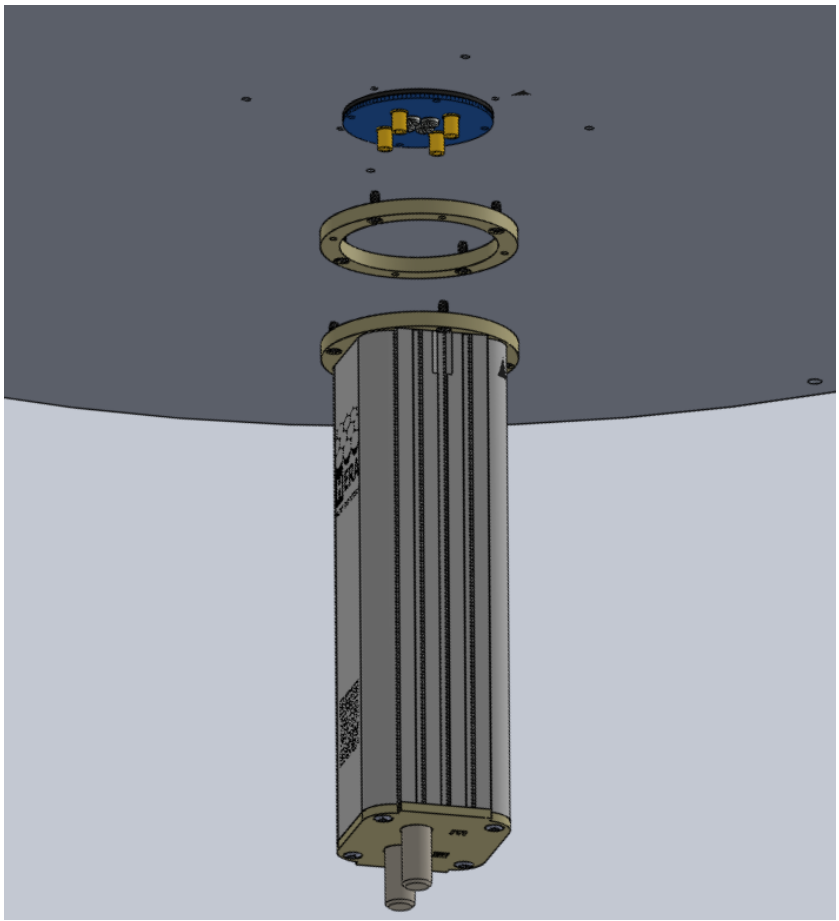

Figure 10: FEM attachment to the antenna via the adaptor ring.

3 Post-amp module overview

3.1 Design and simulation

The PAM circuit was designed to do further filtering and amplification prior to digitisation. The gain of this circuit is nominally 44dB to allow approximately 80dB total gain when including the cable loss. The entire chain was simulated in Keysight Genesys as shown in Figure 11. The PAM has high NF (typically 17dB) due to the input loss, however the effect on the receiver temperature is minimal as described by the Friss noise formula. The majority of the blocks shown in Figure 11 are measured not simulated S-parameter data. As before, the input is defined as a differential port with the impedance of the antenna.

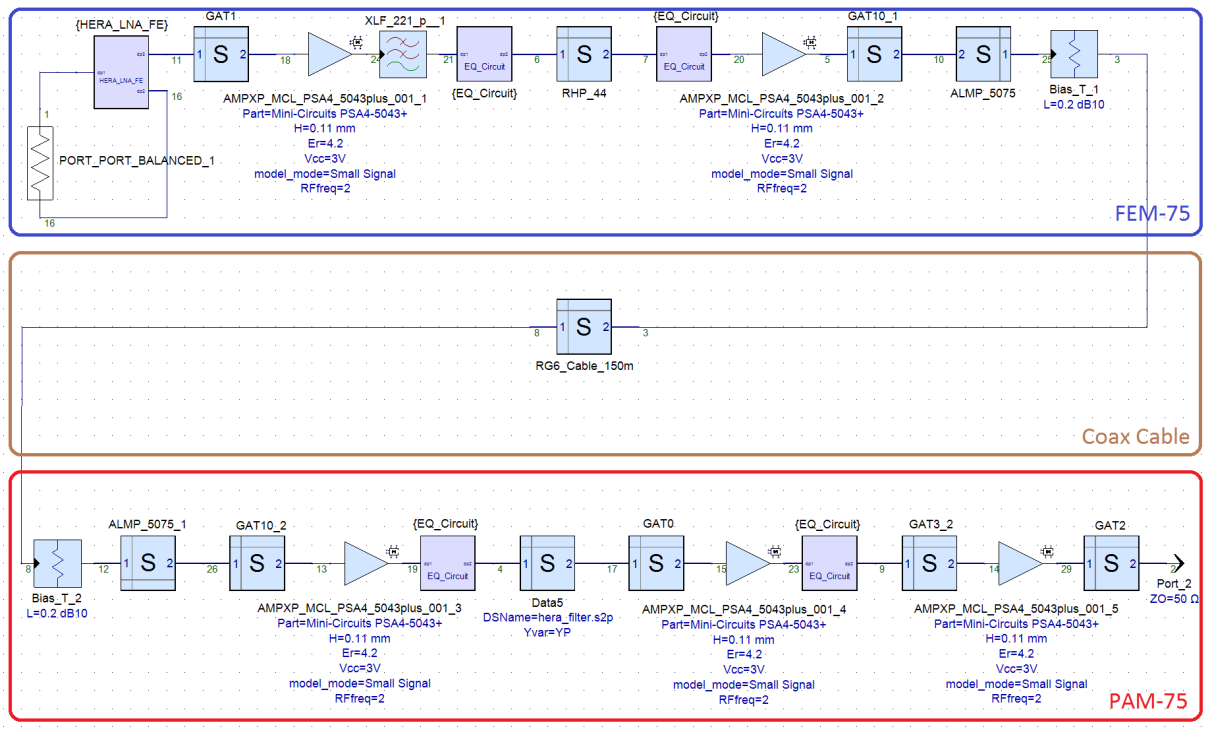

Figure 11: Simulation of entire RF signal chain in Keysight Genesys.

A schematic of the PAM-75 circuit is shown in Figure 12. The inputs for each polarisation are F-type (75Ω) and the output to the digitiser (ROACH boards) is SMA.

A 9-order low pass filter circuit was designed to carry out the anti-aliasing filtering prior to digitisation. The filter is based on a Cauer-Chebyshev design and was simulated in Genesys using Modelithics substrate scalable components. The filter was designed for a roll-off of -3dB at 210MHz, -27dB at 250MHz and -58dB at 290MHz. The latter is the flip response at 210 MHz if sampling at 500 Msps. Only one prototype of the filter was built and tested. It met the specifications very well as shown in Figure 13.

In the schematic shown in Figure 12, there are three stages of amplification in the PAM, using the same gain blocks described before (PSA4-5043+). The nominal output compression point (1dB) of the PSA4-5043+ when running at 3.3V can be increased by +3dBm when fed with 4.5V according to the datasheet. This was therefore implemented to improve all inter-modulation distortion points. Also, the PAM output has ESD protection.

3.2 PCB and rack housing

The dual polarisation PAM PCB is similar to the FEM, however it contains 6 layers instead of 4. This permits more flexibility in the signal routing especially since we wanted to have input and output routed to the same edge of the PCB. The layer stack-up is signal-ground-power-power-ground-signal. The final assembled PCB (top layer) is shown in Figure 14. As with the FEM, a large ground track separates the two polarisations in order to improve cross-talk to a level of -50 to -60dB.

Each PAM is housed inside a Schroff shielded 5HP rack enclosure, thus allowing up to a maximum of 16 modules to be housed inside a 19" 3U rack. Since each module is dual polarisation, a rack can then serve 16 antennas. This was designed to fit within the current receiverators in the field. The final housing inside the rack and outside is shown in Figure 15. One of the advantages of this design is that modules can easily be removed and replaced if need-be.

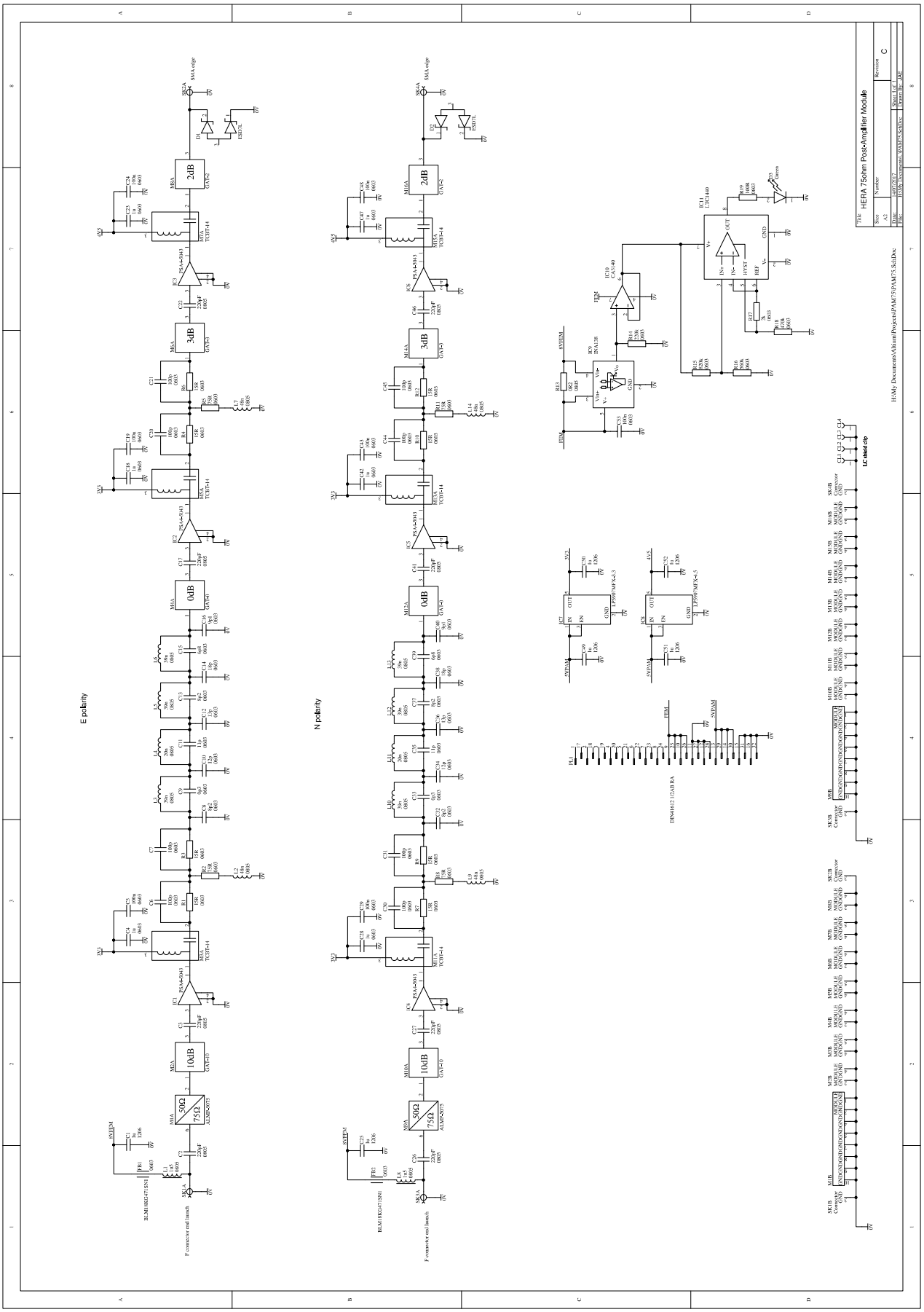

Figure 12: Post-amp module schematic (E and N polarisation).

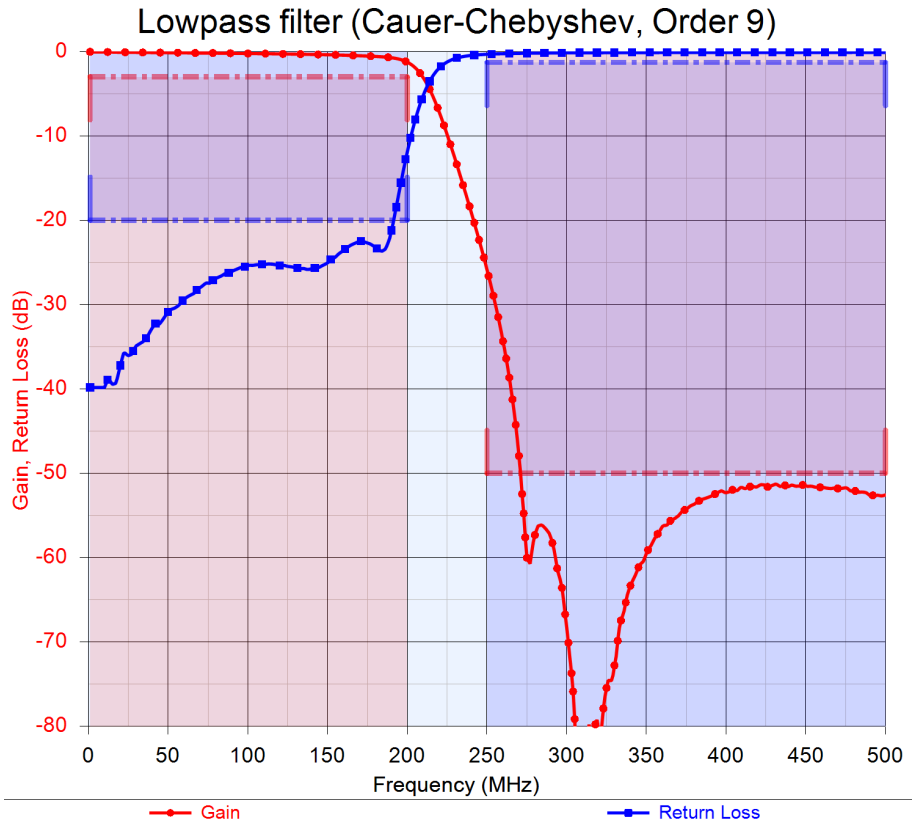

Figure 13: Response of low-pass anti-aliasing filter.

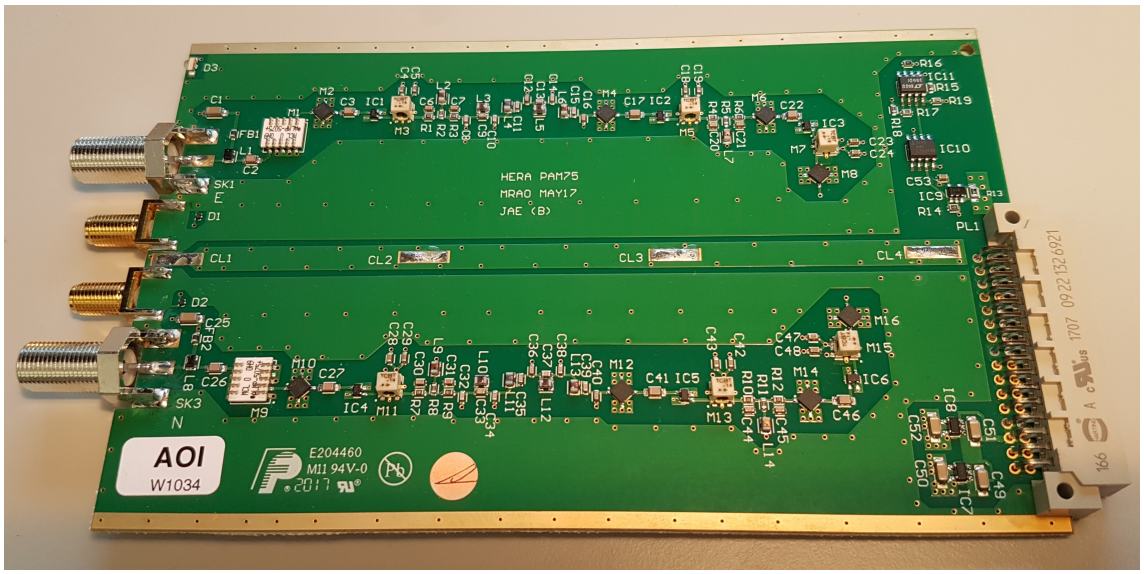

Figure 14: Post-amp module PCB.

Each PAM rack has two low noise switch-mode PSUs, a 5V supply for the PAM internal power and an 8V supply for the FEM line power. External switches at the front of the rack are used to power the rack, then the FEMs. The two voltages are fed via a back-plane to each module. On the PAM, LDOs produce 3.3V and 4.5V on the board for the aformentioned amplification stages. Per 16 antennas (rack), the current rating is approximately 6.4A for the FEMs and 3.6A for the PAMs.

The FEM line power is connected to a current sense circuit on the PAM shown on the bottom right-hand side of Figure 12. This detects the current consumption. If this is above 330mA (for both polarisaions), then a PAM LED will turn on indicating that the attached FEM is being powered, otherwise if the LED does not light it indicates a problem with that FEM, the cable or possibly the PAM itself.

An important consideration is that the 8V FEM line power is connected directly to the PSU via the backplane

Figure 15: Post-amp module housing and rack.

and therefore there is no protection in case of a short. This is a minor oversight which could be better controlled in the next version of the receivers. It is therefore recommended that the F-cables are securely connected at both ends before turning on the FEM line power. In the event of an accident, if the FEM F-type terminal(s) are shorted then the 0805 chokes (Coilcraft 0805AF-152XJRB, 1.5uF, 390mA) on the PAM units shown in Figure 12 will burn out. However, it should be noted that these are easily replaceable. With proper handling of the equipment, this will not occur in the field.

As with the FEM, each PAM is labelled to indicate E and N polarisations and inputs and outputs as well as having a unique Data Matrix code. The data for each module is also made available at hera.mrao.cam.ac.uk.

4 Measurement setup and results

A wide range of laboratory measurements were carried out on both the FEM and PAM units. The majority of these measurements were done with a Keysight PNA-X which is a highly re-configurable 4-port VNA. The general modes of use were standard 3 and 4 port s-parameters, 2-port noise parameters and intermodulation power measurements. These are described in the following sections. All the measurements presented here were validated against simulations and showed good agreement, with typically up to 1dB difference on s-parameters and up to 0.2dB for noise measurements.

The devices under test are considered high gain. This is especially true of the FEM which has a gain of 46dB, however when excluding the output padding (10dB attenuator and resistive transform), the gain is approximately 62dB meaning very low input power levels should be used in testing, typically -55dBm. To avoid noisy data, especially for noise parameter measurements, all of the results presented here were collected using an in-house EMI/RFI shielded box designed to work from DC to 18GHz with more than 70dB absorption at the HERA frequencies. The internal dimensions of the box are 360 x 360 x 160 mm which is sufficient to hold a FEM or PAM or both. All connections are made through the bulkhead including the DC power which goes through a 1.9 MHz low pass filter. Typically for the calibration setup, the reference planes where made inside the box at the end of additional high quality (low phase distortion) coax cables which were 30cm long. The calibration included any bias-Ts used to feed power to the FEMs. The typical arrangement is shown in Figure 16 along with the PNA-X.

For all FEM measurements a test adaptor was used which resembled the antenna mating board and converted the PowerSnap to SMA female [3]. Due to the differential input, some data was collected using a low-loss hybrid (0°/180°) splitter at the input (model ZFSCJ-2-1+ from minicircuits). When it was attached to the FEM, it made a strong galvanic contact around the circumference of the flange. We found the area around the PowerSnap input connectors to be very sensitive and hence why this module was developed for reliable measurements. Figure 16 also shows the test adaptor connected to two splitters (E and N channels).

The splitter was used when only 2-port measurements were required such as noise parameters (differential noise parameters not available) and intermodulation power measurements. It was also useful for measuring cross-talk between each polarisation on the board (4-port measurements). For each case, the splitter was de-embedded. In all modules produced, 3-port measurements of each FEM polarisation (E and N) were made separately. All data made available for the FEMs is 3-port since this offers the most flexibility in using it for EM simulations or standard RF analysis. The 3-port data can easily be converted to 2-port using a lossless balun in RF packages such as Genesys. When measuring the PAMs, the setup was easier since all inputs and outputs are single ended. Figure 17 shows the port arrangements when making the measurements.

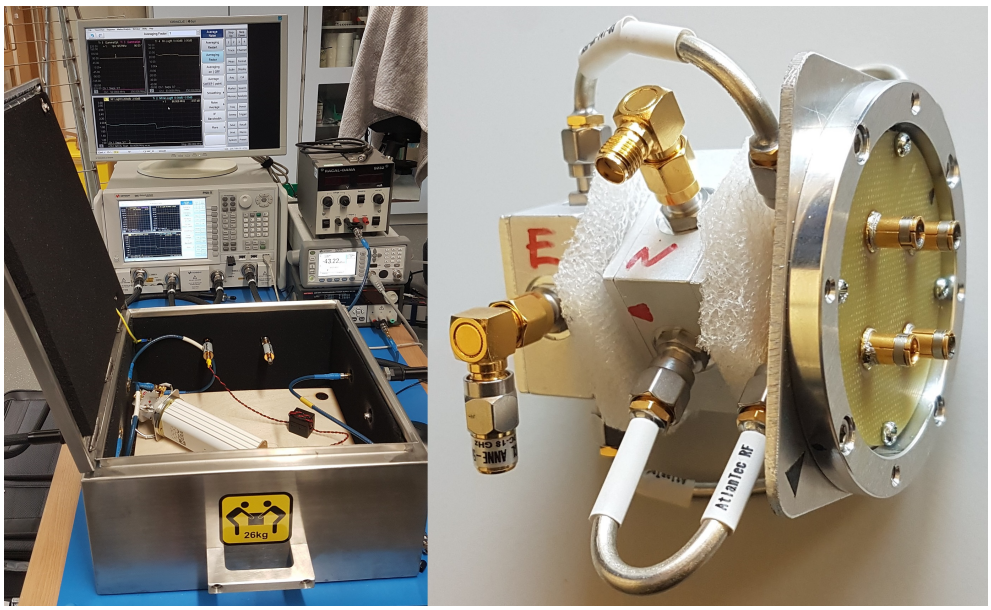

Figure 16: Shielded test enclosure and PNA-X (left), test adaptor and hybrid splitter based on ZFSCJ-2-1+ used for FEM measurements (right).

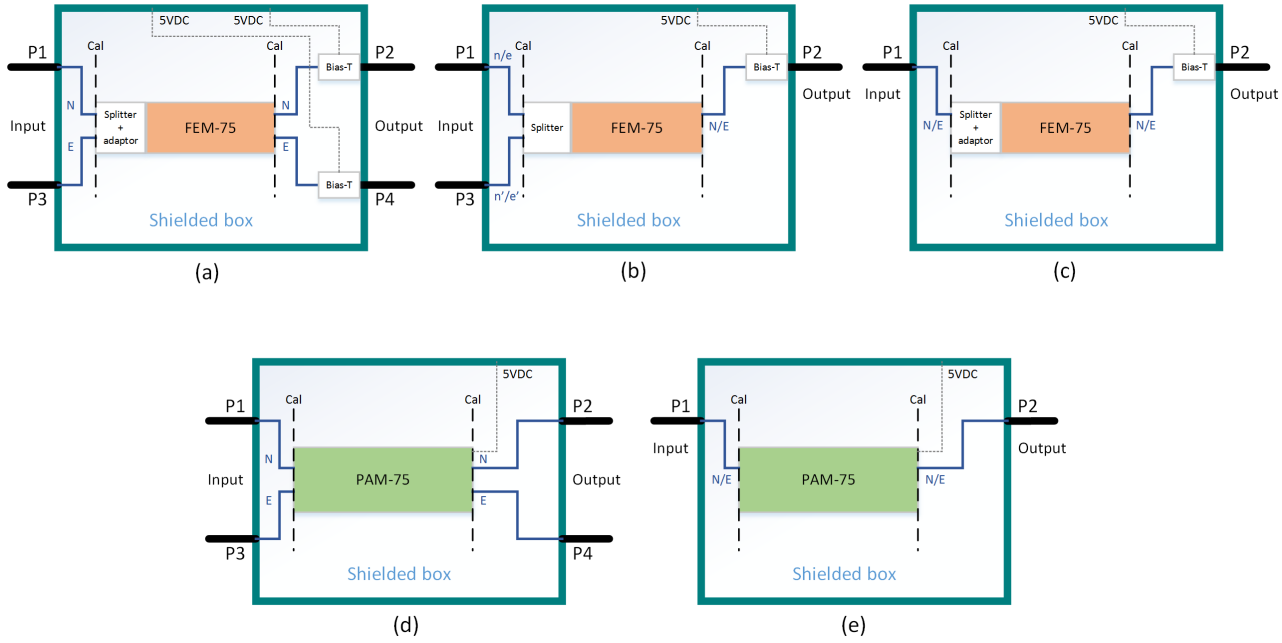

Figure 17: PNA-X port arrangements for different measurements.

4.1 S-parameter data

S-parameter measurements were made of the FEMs and PAMs in every configuration shown in Figure 17. Figure 18 shows the results for the FEMs based on configuration (a) and Figure 19 shows the results for the PAMs based on configuration (d). Furthermore, Figure 20 shows the full system response when including the 150m twin Belkin (RG6) cable used on site. The loss of the splitter has been de-embedded from the results.

The measurements shown were carried out with the PNA-X as described in the previous section. The PNA-X was typically calibrated using the following parameters:

- Start Frequency = 10MHz, Stop Frequency = 500MHz
- Number of points = 491 (one point per MHz)
- IF bandwidth = 500Hz with averaging factor = 15
- Power (ports 1 and 3) = -30dBm, Power (ports 2 and 4) = -20dBm

Due to the high gain of the devices, after calibration, the input power (ports 1 and 3) were reduced to -55dBm, -40dBm and -70dBm for FEM, PAM and the full chain, respectively. These are all lower than the input compression points as will be shown later. A summary of the results will be shown in the final section. It should be noted that all the results shown here have a reference impedance of 50Ω. When taking into account the impedance of the antenna, the ripple on the forward gain in the 100-200MHz band is ±1dB similar to that shown in Figure 4.

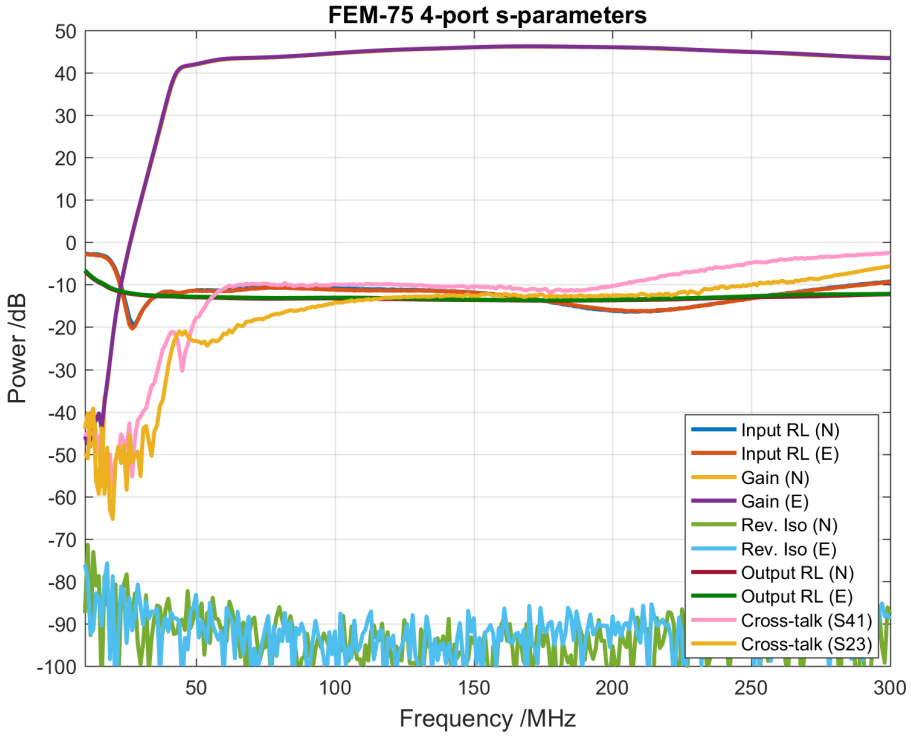

Figure 18: FEM-75 4-port s-parameters.

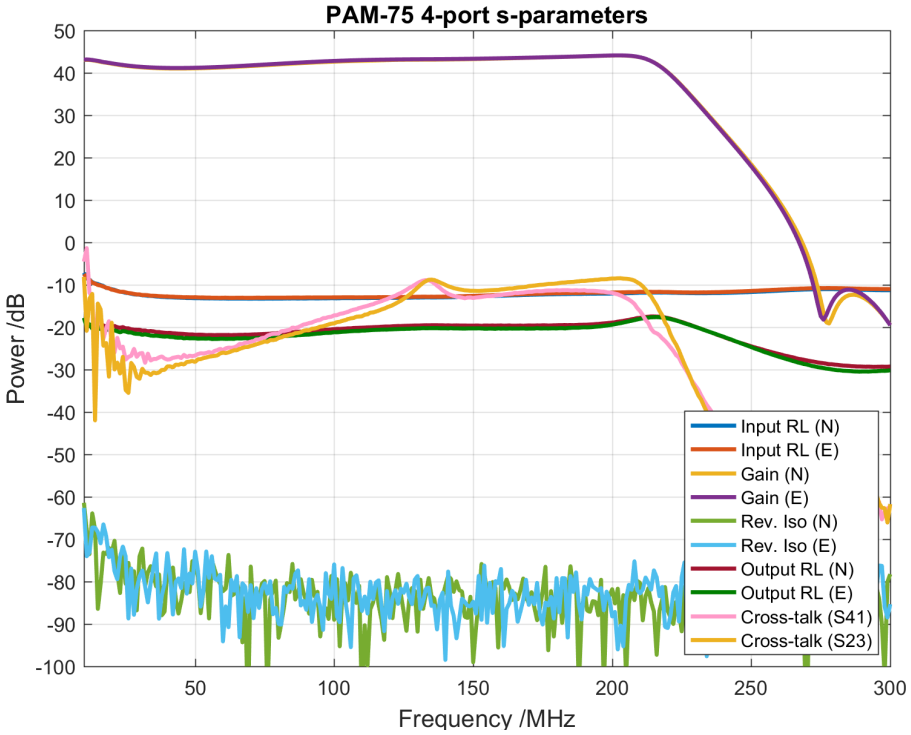

Figure 19: PAM-75 4-port s-parameters.

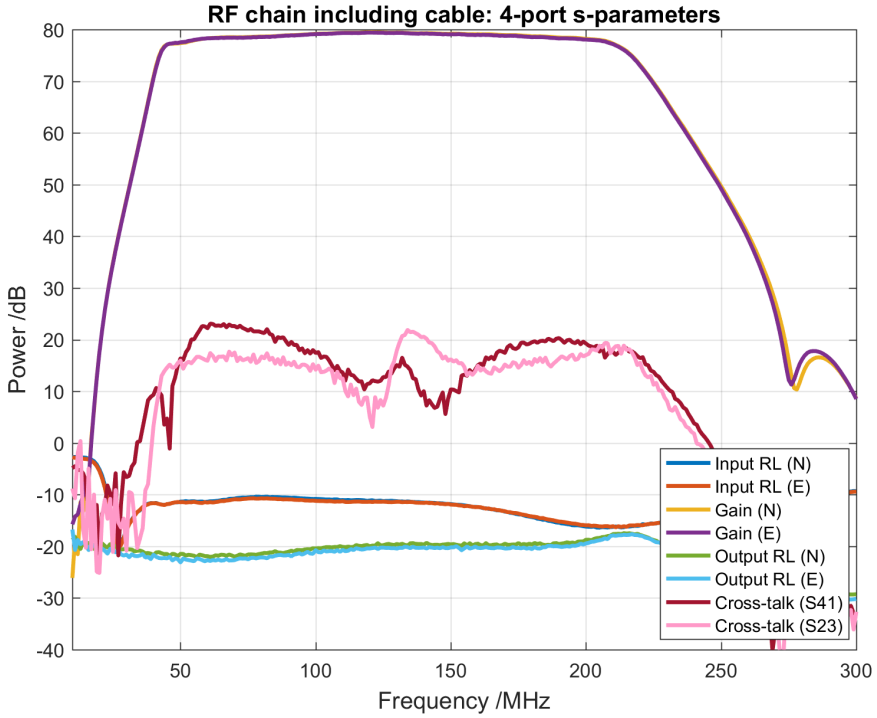

Figure 20: HERA RF chain s-parameters (FEM+cable+PAM).

4.2 Match performance

As described earlier, the match between the antenna and front-end given by analysing VSWR or mismatch loss is critical for the performance of the HERA system since this has a direct impact on the antenna delay spectrum. Figure 5 showed the simulated mismatch loss of different optimised networks. In Figure 21, we show mismatch loss from measured data comparing the original system with the new system.

The interesting result here is that the match performance is considerably better than the simulated results. Whilst the frequency of the peaks do correspond, the level of the peaks are lower. The difference here between the original and new system is also considerable, even when comparing the 110-190 MHz band, where the average mismatch loss is 1.27dB and 0.34dB for the original and new systems, respectively. EM simulations of the full system should be carried out to see what impact this has on the delay spectrum profile.

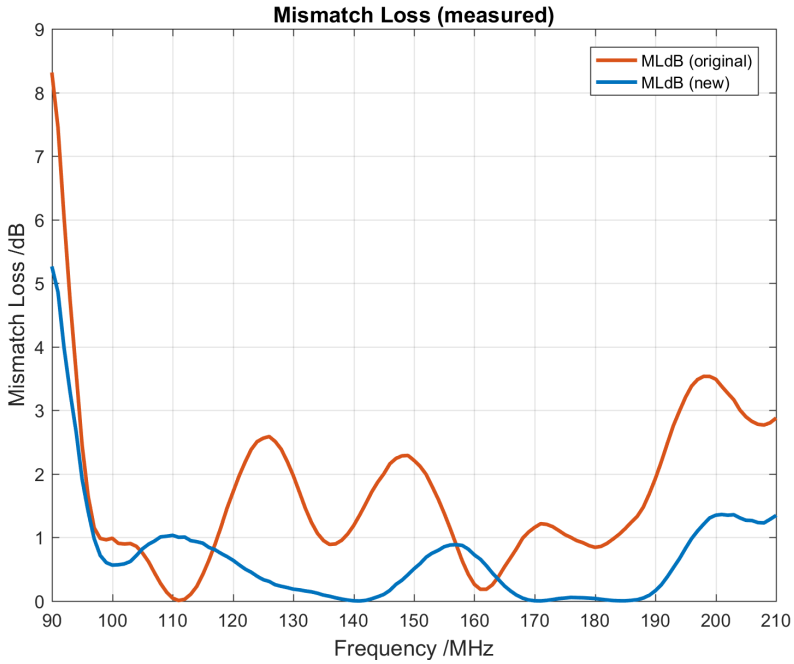

Figure 21: Measured mismatch loss comparison between new and original system.

4.3 Receiver temperature and scan sensitivity

One of the critical design parameters for the HERA RF system is the receiver noise figure (NF) given in dB or receiver temperature, T_{rec}, given in Kelvin. At low frequencies, the average sky brightness temperature is dominated by the synchrotron emission which is approximately 1000K at 100 MHz reducing to approximately 150K at 200 MHz. Ideally for HERA, we would like to be sky-noise dominated for the entire band. However, whilst this is just achieved by the current receiver system, we aimed to significantly improve this especially at the higher end of the band where we could have a large impact on sensitivity.

Using our PNA-X, we carried out 2-port noise measurements of the FEM and PAM using configurations (c) and (e) of Figure 17, respectively. We used a frequency resolution of 1MHz with 7 points taken around the smith chart and 25 noise averages. In the case of the FEM, the balun response was de-embedded from the results. Figure 22 shows the difference in receiver temperature between the new and original receivers when taking into account the antenna impedance. This is very much in line with the earlier simulations of the front-end. The new system has approximately 70K average lower T_{rec} across the band than the original system.

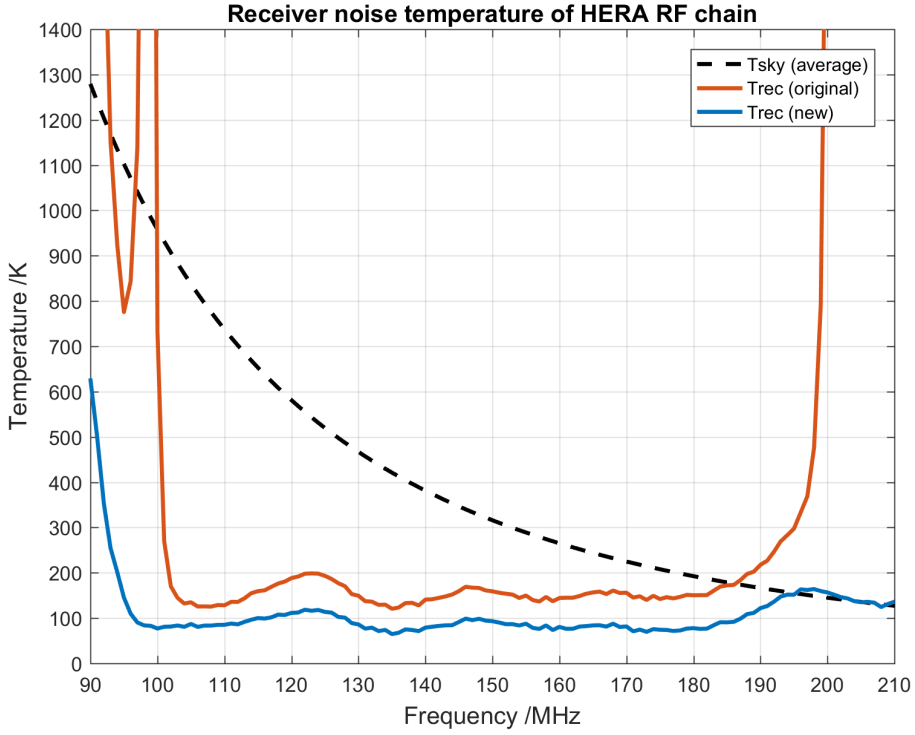

Figure 22: HERA receiver temperature.

In order to understand the effects on the sensitivity, simulations were done using Xarray [4], a tool developed in 2011 for the SKA community [5] to compute the response of array systems (as described in [6]). The tool uses both a spectral model of the sky as described in [7] and the Haslam 408MHz all-sky survey [8] to compute antenna temperature, T_A as well as sensitivity. Here, we defined the sensitivity metric as effective area, A_{eff} divided by system temperature, T_{sys} described by

$$T_{sys} = \eta T_A + \eta(1 - T_{amb}) + T_{rec} \tag{4}$$

where η and T_{amb} are the antenna radiation efficiency and the ambient temperature, respectively. T_A is given by integrating the antenna beam, $|F|^2$, over the entire sky with brightness temperature, T_{sky} as a function of frequency, ν

$$T_A(\nu) = \frac{\oint\!\!\oint_{4\pi} T_{sky}(\nu,\Omega)|F(\nu,\Omega)|^2 d\Omega}{\oint\!\!\oint_{4\pi} |F(\nu,\Omega)|^2 d\Omega} \tag{5}$$

To carry out the analysis, HERA simulated beam patterns were loaded into Xarray and the sensitivity was calculated using both a spectral sky model and the Haslam map. The beam data was simulated in CST by Nicolas Fagnoni [9] and is available on the HERA wiki. Figure 23 shows the HERA sensitivity as a function of frequency, where there is up to 30% increase in sensitivity due to the new receivers.

Simulations were also carried out using the Haslam map. In Xarray, at each point in time, a frequency scaled map of the sky is produced and this is convolved with the beam. In this case the drift scan simulations were done assuming the centre of the HERA antenna to be 30°43'17"S, 21°25'41"E. The frequency and time resolution is 1MHz and 10 minutes respectively.

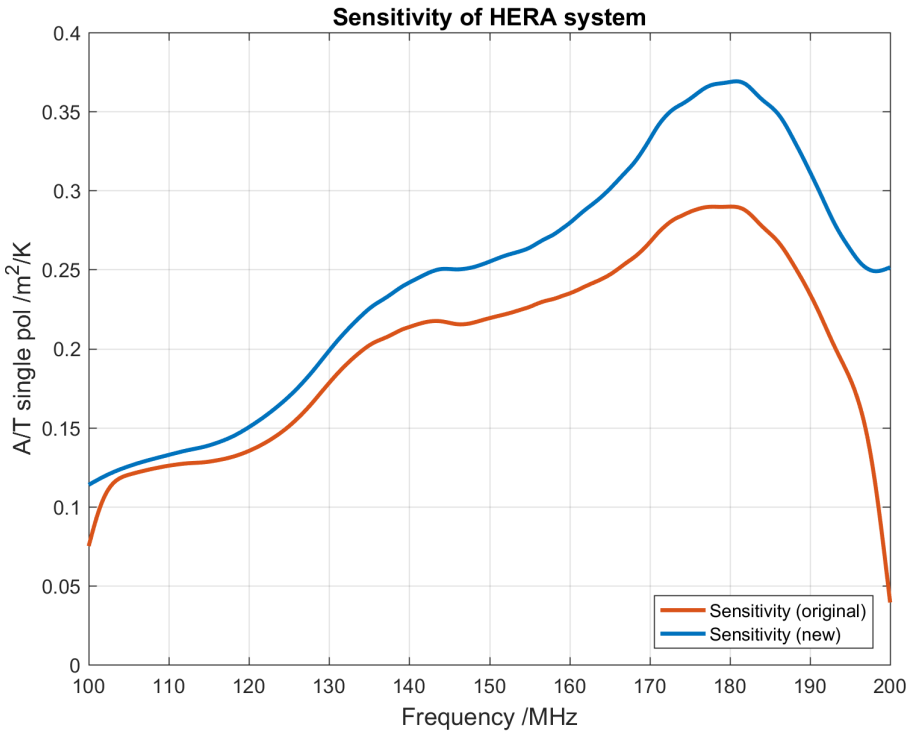

Figure 23: HERA sensitivity comparison.

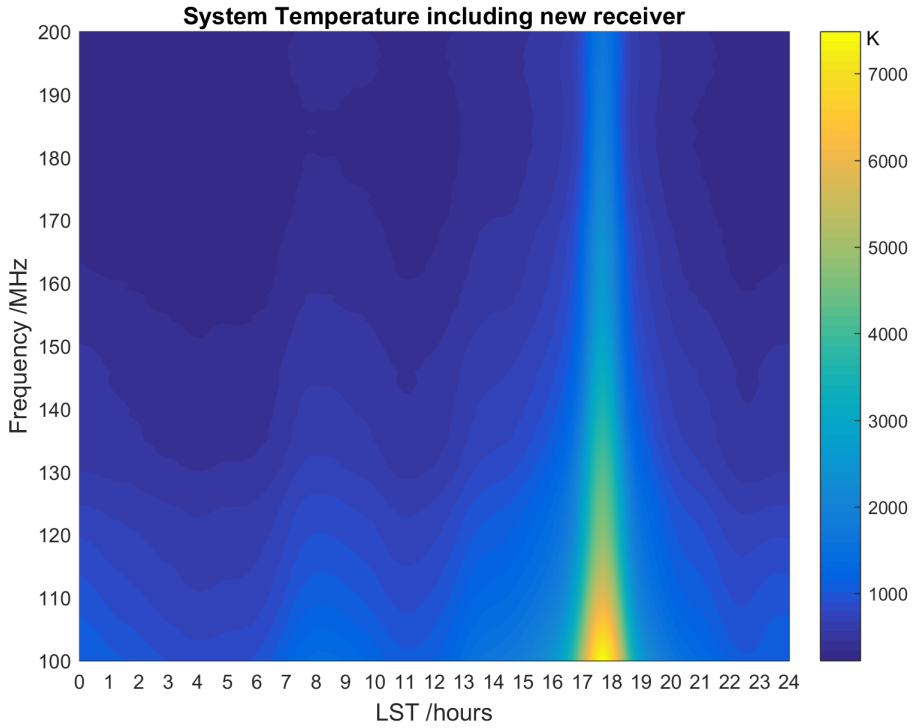

Figure 24: HERA scan system temperature with new receiver.

The results presented here are based on measurements of the receiver system and antenna S11 and simulations of the beam, however they do not take into account the RFI on site which degrades the sensitivity. As shown later on, this is particularly an issue from 106-125 MHz, where the RFI level is significant.

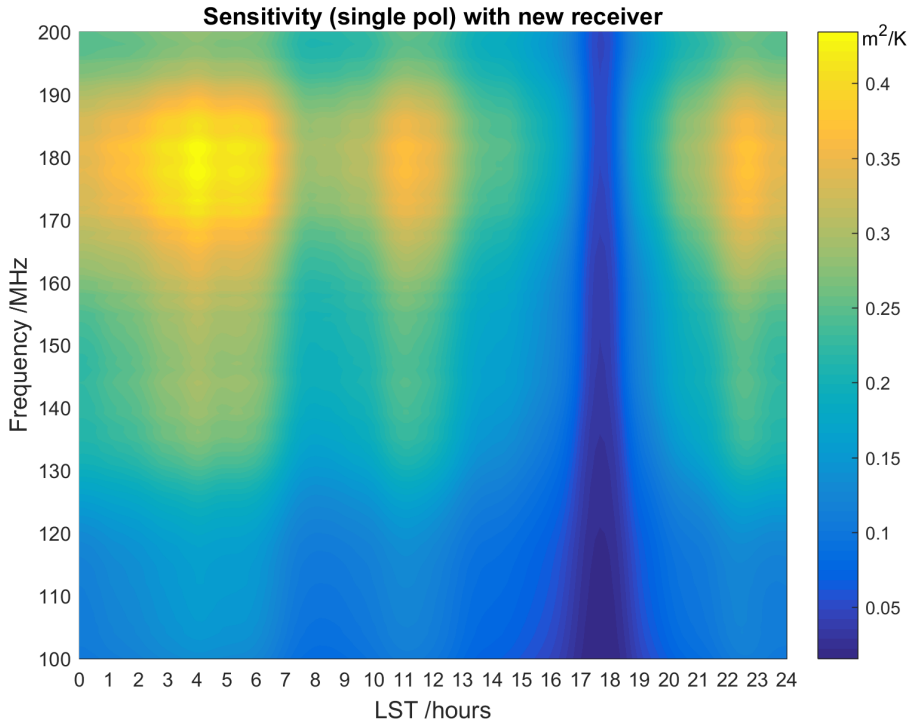

Figure 25: HERA scan sensitivity with new receiver.

4.4 Intermodulation and compression

Dynamic range is defined as maximum input level/minimum input level, where minimum level is such that the output signal to noise ratio is sufficient and maximum level is such that the effects of non-linearity are less than or equal to the noise (e.g. third order harmonics are less than or equal to the noise).

This is normally defined by the system IP3 and IP2 which are the third and second order harmonics, respectively, although since IP3 is reached first, it is the term that most determines dynamic range. These terms are defined such that if two tones are inputted into the system with frequencies f_1 and f_2, we would have third order harmonics at $2f_2 - f_1$ and $2f_1 - f_2$ and second order terms at $f_2 + f_1$ and $f_2 - f_1$.

Another important metric is compression. Generally amplifiers maintain a constant gain for low-level input signals. However, at higher input levels, the amplifier goes into saturation meaning its gain decreases and the output power level flattens. The 1 dB compression point (P1dB) indicates the power level that causes the gain of the system to drop by 1 dB from its small signal value. Sometimes, the 0.1dB compression point is also determined as being the point where the gain drops by 0.1dB and has therefore just started to saturate.

We used the PNA-X in configurations (c) and (e) of Figure 17 to measure the intermodulation distortion (IMD). The mode used was "IMD Spectrum" which essentially inputs 2-tones into the system and displays the spectrum at the output. This method whilst being accurate can only be done at spot frequencies. Here we present results for 150MHz which is the centre of the HERA band. Although, these results can be tuned for different frequencies simply by using the gain profiles shown in the s-parameters. A summary of the results will be presented later.

We used the PNA-X to measure input and output powers of the principle tones (P1), the third order tones (P3) and the second order tones (P2). From this we could determine the various IMD points. It was critical when measuring any of the aforementioned tone powers to ensure the system was not saturated and that we were not trying to measure power levels close to the noise floor of the PNA-X, otherwise this could skew the results. For P2 and P3, this meant measuring at low power levels to determine their slopes. In Figures 26,27,28, and 29 we show the measurements of the FEM, PAM and full chain (new and original), respectively. Here we can see that the IMD performance is improved with respect to the original system. For example, the input 1dB compression point (IP1dB) is -68.8dBm for the new system and -82.75dBm for the original system.

In January 2017, RFI measurements were collected for each polarisation of a HERA antenna on site. The measurements were carried out over a 30 minute window using 10kHz resolution bandwidth. The results are shown in Figure 30. The measurements were made with a balun and cable and have been de-embedded from the data. Although it is clear that we had limited dynamic range from the noise floor of the spectrum analyser used (Keysight FieldFox), the RFI shows several peaks with that of 125MHz (-76dBm) being most prominent. From this data alone, we can determine that most likely all of the original receiver systems are well into compression although 10dB away from the IP3 point.

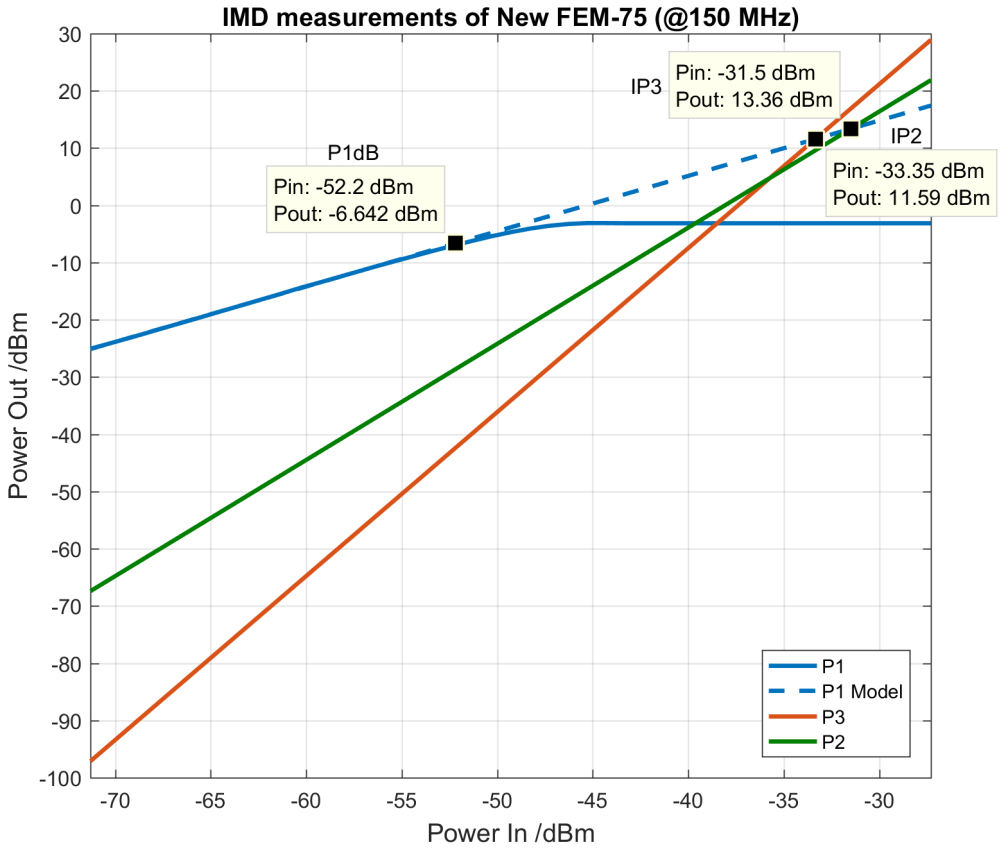

Figure 26: FEM-75 IMD measurements.

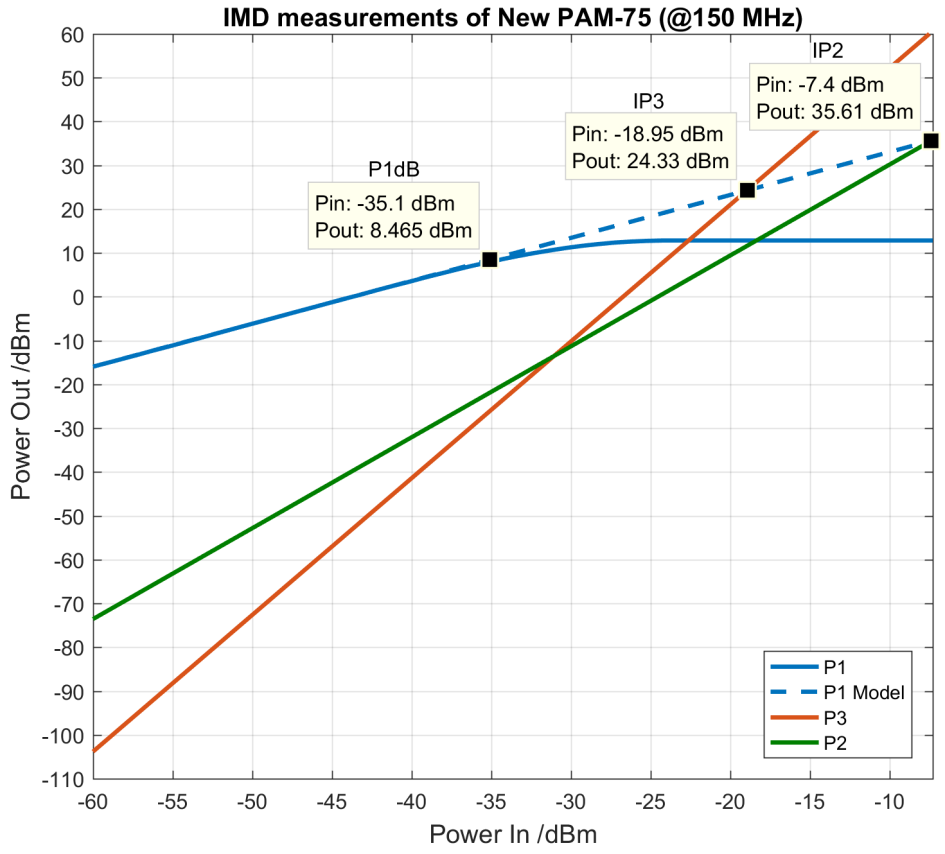

Figure 27: PAM-75 IMD measurements.

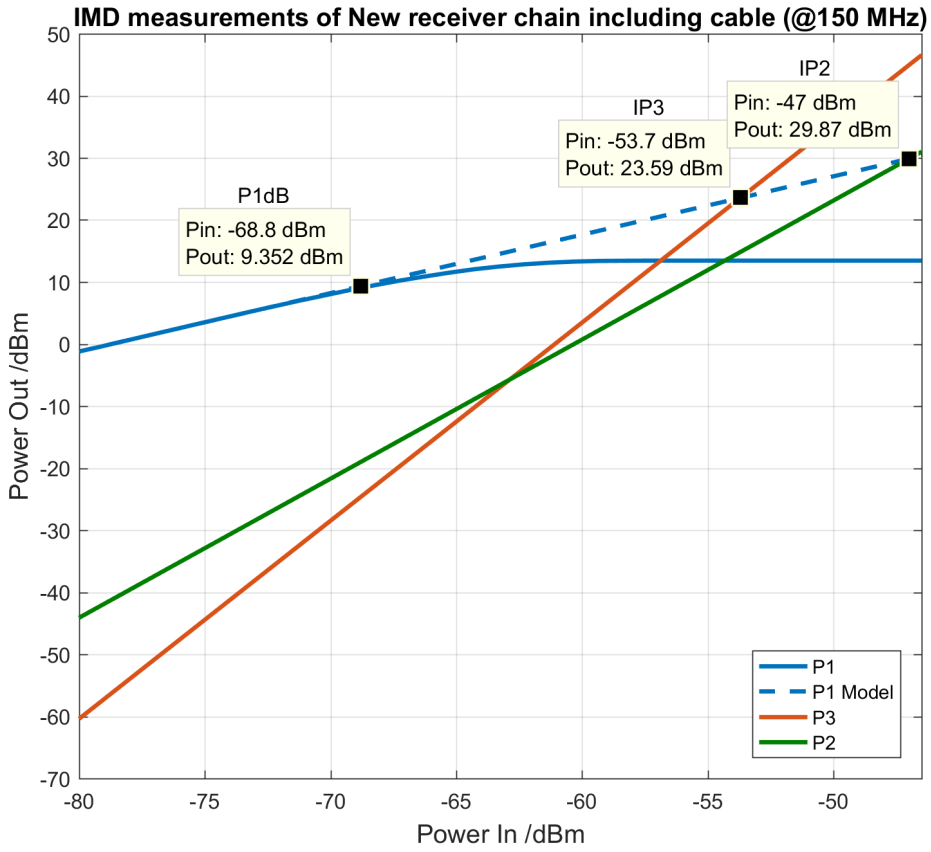

Figure 28: IMD measurements of new receiver chain including cables.

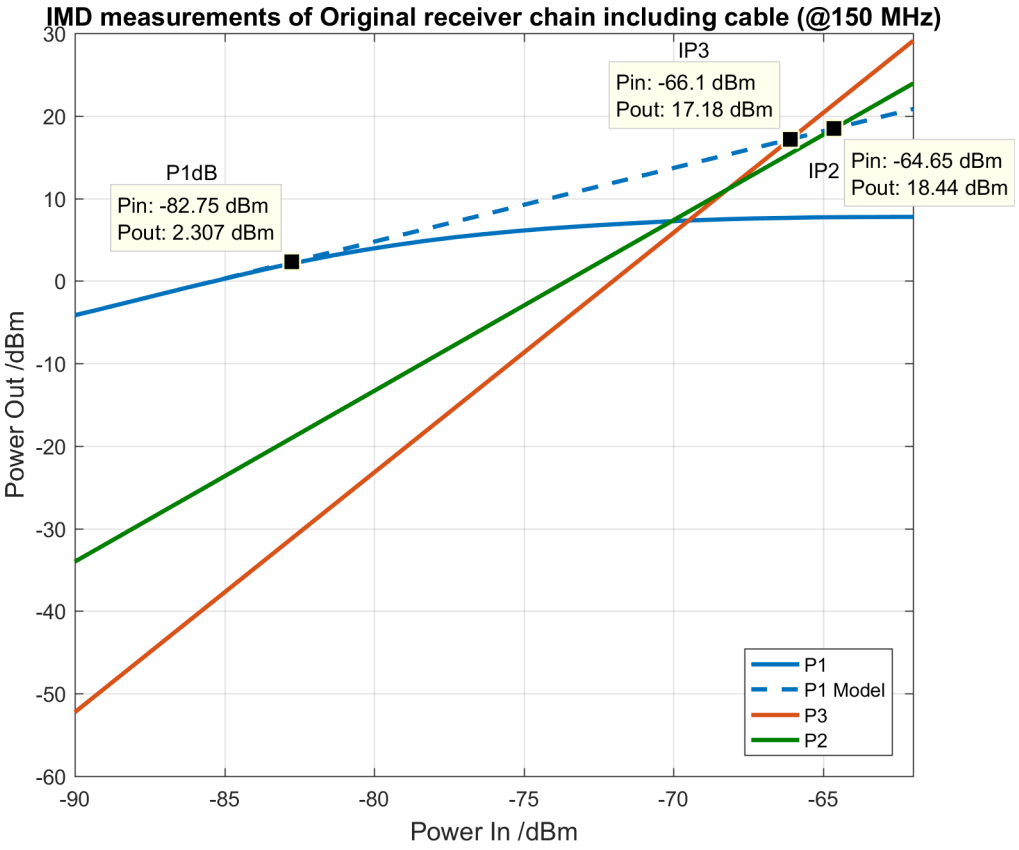

Figure 29: IMD measurements of original receiver chain including cables.

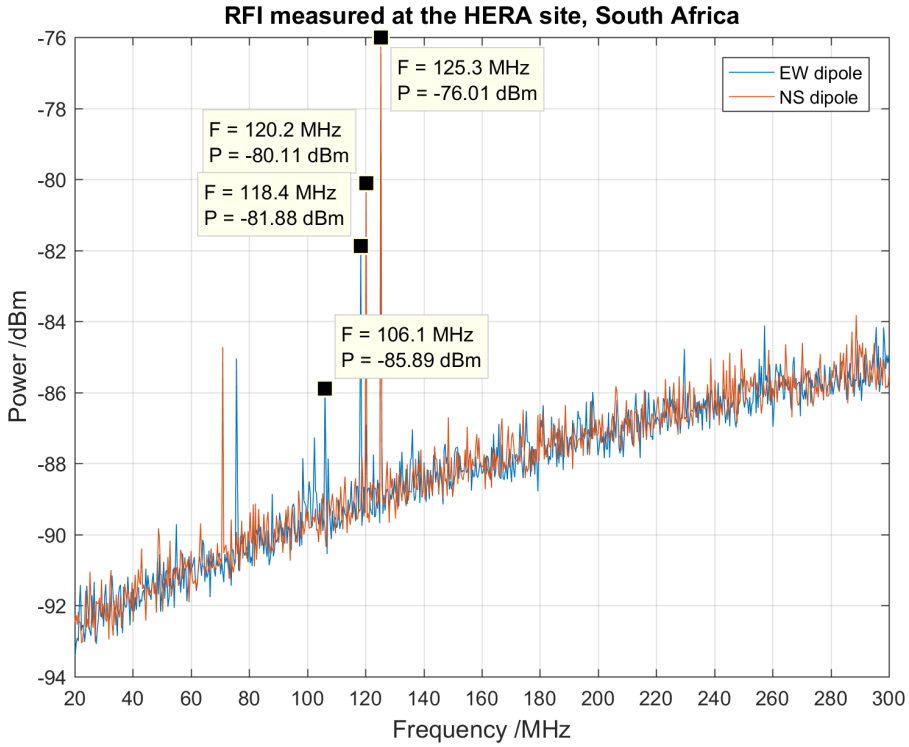

Figure 30: RFI measurements carried out in the Karoo with a HERA dish (January 2017).

4.5 Stability and environmental performance

Stability, in referring to active systems (amplifiers), refers to their immunity to causing spurious oscillations. This is a rich subject and there are various parameters which could be analysed to determine with certainty if an amplifier can oscillate. The criteria we use is unconditional stability, which refers to a network that can connect to any possible impedance on the Smith chart from the centre to the perimeter (up to $\Gamma = 1$) at any phase angle and not oscillate. Here we use the K-factor, which if greater than 1 implies the system is unconditionally stable. The definition is as follows in a 2-port system

$$K = \frac{1 - |S_{11}|^2 - |S_{22}|^2 + |\triangle|^2}{2|S_{21}S_{12}|} \tag{6}$$

where

$$\triangle = S_{11}S_{22} - S_{12}S_{21} \tag{7}$$

Other parameters such as maximum available gain, G_{MAX} (when $K > 1$) have also been looked at but are not discussed further here. To do the K-factor analysis, we used data corresponding to configuration (b) and (e) of Figure 17. For the FEM, we used a lossless balun module in Keysight Genesys to compute 2-port K-factor from 3-port s-parameters. Generally calculating K-factor for high gain devices can be difficult since the power levels have to be low and this can make the results noisy. We used standard data which has been averaged for 15 sweeps at an IF bandwidth of 500 Hz. Figure 31 shows the results for the FEM and PAM modules (new and original). All modules as expected are considered unconditionally stable as K is greater than 1.

As part of the measurements, we also examined effects due to temperature variation for the FEM since this module is exposed to different temperatures during the day. This was done by placing the FEM inside an environmental chamber and changing the temperature from -10°C to +60°C in 8 hours. Figure 32 shows the variations on the FEM-75 gain as a function of temperature. The current was also examined and found to follow the linear fit $I_{MA} = 0.43°C + 404$.

4.6 Monitoring station at Lords Bridge

A three antenna system has been built at Lord's Bridge, Cambridge for testing the feed designs as well as the receiver system. Currently, one of the HERA antennas is connected to the latest FEM and PAM modules with an equivalent RG6 cable connecting the two. The outputs from the PAM (both polarisaitons) are fed into a real-time spectrum analyser which is used to examine RFI data on site. In the next design phase, more modules will be tested and connected to a high resolution (12-bit) ADC version of the SNAP board already made for the Lord's Bridge system. This will be especially useful for developing the in-situ calibration technique.

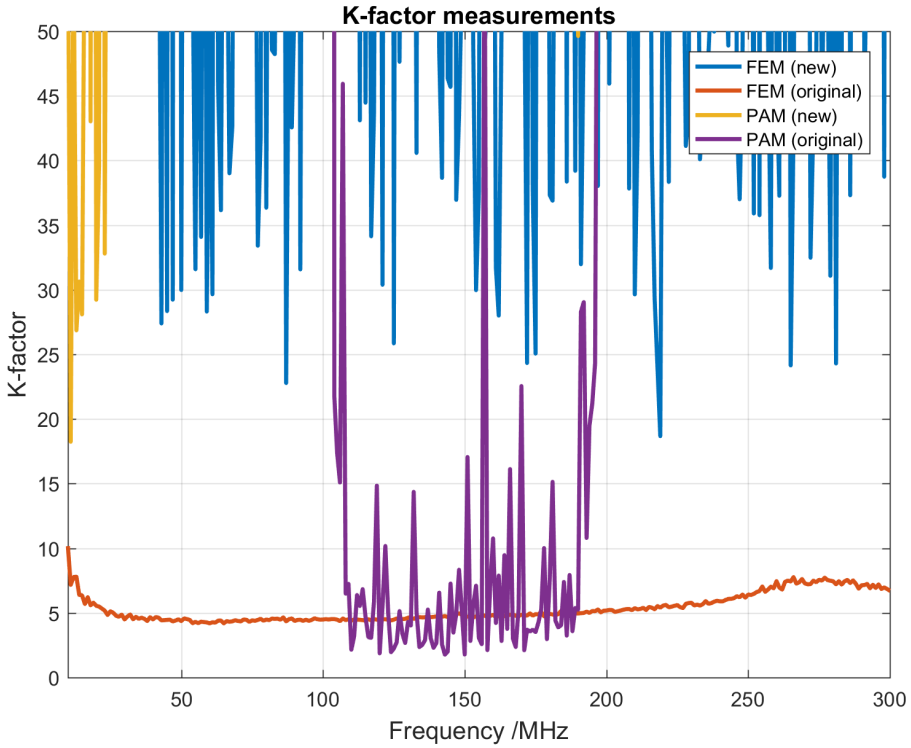

Figure 31: K-factor measurements of receiver system.

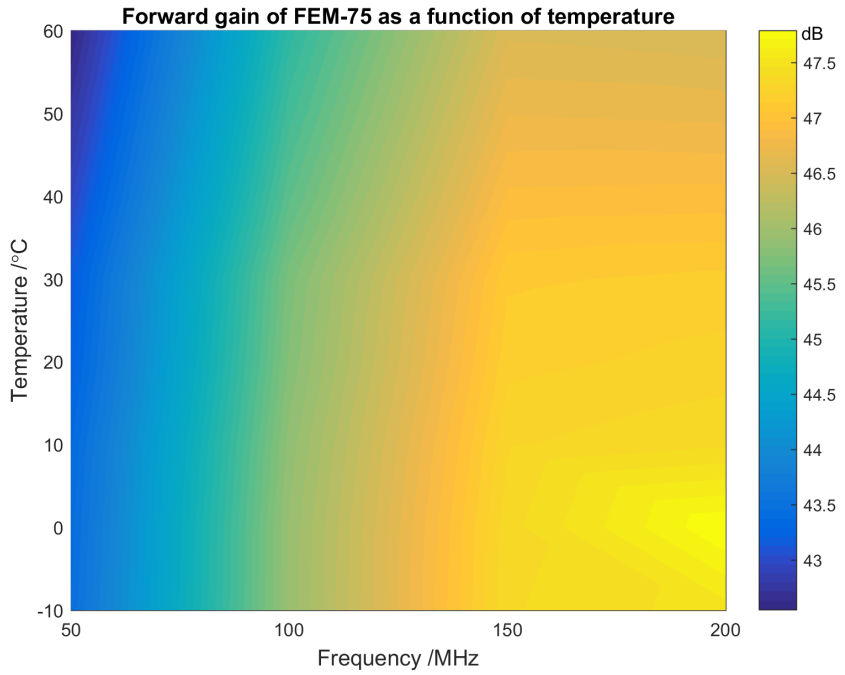

Figure 32: FEM-75 forward gain variation as a function of temperature.

5 Modules and database

A total of 68x FEM-75 and 68x PAM-75 units have been sent to South Africa for deployment at the HERA site. Each module is given a QR code and Data Matrix serial number and label which is unique to the device. For the FEMs, the numbering ranges from 75001 to 75068 and for the PAMs this is 75101 to 75168.

The s-parameters of every single module has been measured by the PNA-X in high resolution. For the FEMs, this is 3-port data (configuration (b) of Figure 17), requiring two files for each module (N and E polarisations). For the PAMs, a single 4-port dataset is available (configuration (d) of Figure 17). These s-parameters are shown in Figure 33 and Figure 34 simply to show the low level of variation from module to module. Typically S-parameter variation of order ±0.5dB is expected. In the case of the PAM, the cross-talk has more variation

due to the fact that this is difficult to measure at low power levels. This still shows a cross-talk range of -50 to -60dB.

Finally, variations were examined by measuring the running current of each device. For the FEMs (both polarisations), this was 397 ±25mA and lower for the PAMs at 227 ±5mA. The FEMs require more power and appear to have more variation in their current draw due to the more power hungry LNA. A full database of all s-parameter data and running currents is available at **hera.mrao.cam.ac.uk**, where each module data can be downloaded or plotted. The QR code printed on the FEMs also points to this website.

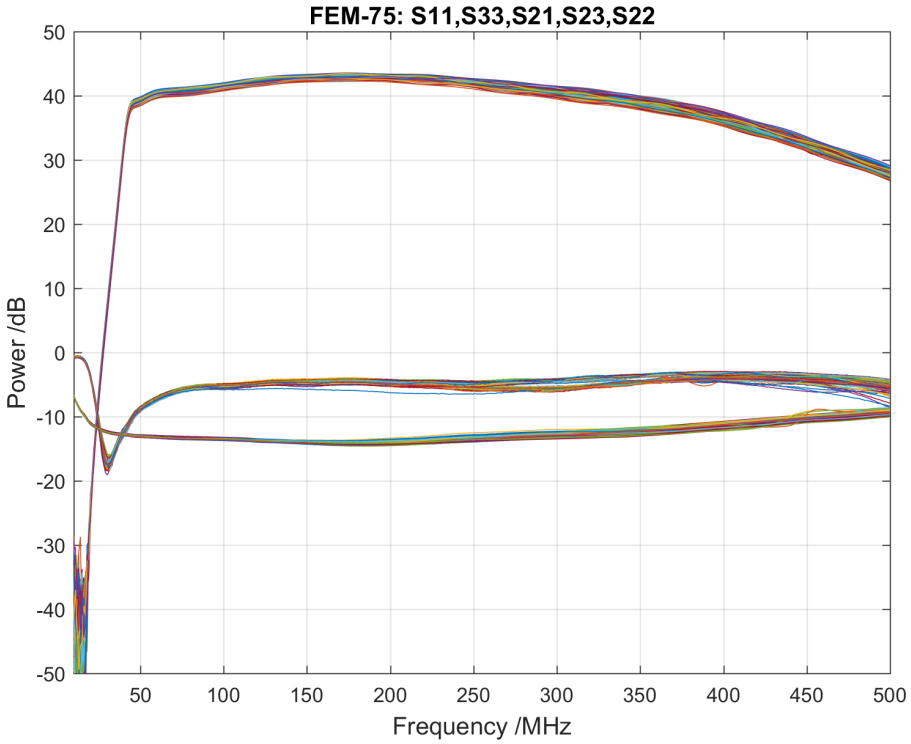

Figure 33: FEM-75: all modules 3-port (N & E) s-parameter data (75001 to 75068).

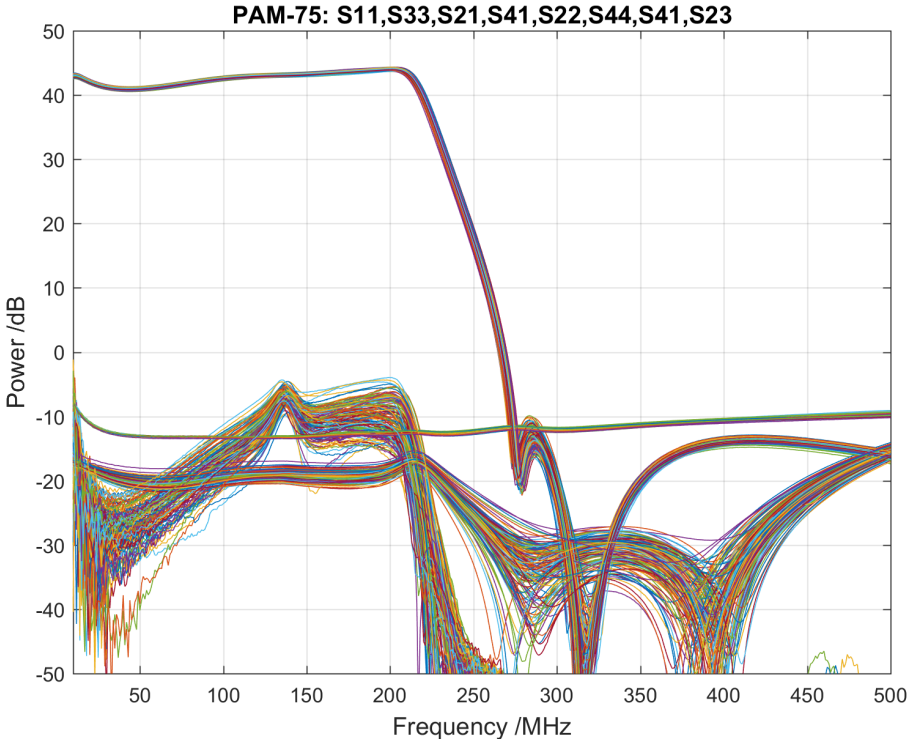

Figure 34: PAM-75: all modules 4-port s-parameter data (75101 to 75168).

5.1 Summary of results

A summary of the end-to-end RF chain parameters (typical) is given in Table 1

Table 1: Summary of RF chain parameters (with respect to 50Ω)

	Frequency (MHz)				
	50	100	150	200	250
Gain (dB)	77.4	79.1	79.2	78.2	49.7
Noise Figure (dB)	1.88	0.91	0.93	0.89	1.15
Input Return Loss (dB)	-10.0	-11.1	-10.2	-10.5	-12.4
Output Return Loss (dB)	-21.5	-20.4	-19.6	-18.7	-24.5
Isolation (dB)	<-100				
Cross-talk (dB)	<-50				
Stability (K factor)	>100				
Input 1dB Compression (dBm)	-67.0	-68.7	-68.8	-67.8	-39.3
Input IP3 (dBm)	-51.9	-53.6	-53.7	-52.7	-24.2
Input IP2 (dBm)	-45.2	-46.9	-47.0	-46.0	-17.5

6 Conclusions and future work

In this memo we have presented the new 75Ω system for HERA encompassing the front-end and post-amp modules. We used a PNA-X to carry out most of the measurements of each module, namely s-parameters, noise parameters, intermodulation distortion and stability. The results have shown improvements in all areas including matching to the antenna. The receiver noise temperature has decreased by an average of 70K meaning up to 30% more sensitivity. The frequency band has been extended by up to 40MHz and there is improvement in the compression and intermodulation points which is required due to the increasing RFI levels on site. Furthermore, the new housing and PCB design should reduce maintenance time and increase reliability.

In the next phase of the design, we would like to incorporate what we have learnt in all the aforementioned areas and get improved performance from the new feeds which are going to be deployed in Q3 2018. Much of the prototyping can now happen at the Lord's Bridge, Cambridge site. We would also like to employ other simulations to help understand the trade off in terms of match and noise performance and therefore achieve the best possible balance.

References

[1] D. R. DeBoer, A. R. Parsons, et al. Hydrogen Epoch of Reionization Array (HERA). *ArXiv e-prints*, June 2016, arXiv:1606.07473 [astro-ph.IM].

[2] A. R. Parsons, D. C. Backer, et al. The Precision Array for Probing the Epoch of Re-ionization: Eight Station Results. *AJ*, 139:1468–1480, April 2010, arXiv:0904.2334 [astro-ph.CO].

[3] S. Carey, J. Ely, and N. Razavi-Ghods. RF installation of new HERA receiver system. *HERA technical report*, July 2017.

[4] `https://sites.google.com/site/xarraytool/`.

[5] `http://skatelescope.org/`.

[6] N. Razavi-Ghods, E. de Lera Acedo, A. El-Makadema, P. Alexander, and A. Brown. Analysis of sky contributions to system temperature for low frequency SKA aperture array geometries. *Exp. Astron*, 33:141–155, March 2012.

[7] G Cortes Medellin. US-SKA Technical Memo 95: Antenna Noise Temperature Calculations. *SKA-Memo*, 1995.

[8] C. G. T. Haslam, C. J. Salter, H. Stoffel, and W. E. Wilson. A 408 MHz all-sky continuum survey. II - The atlas of contour maps. *AAPS*, 47:1, January 1982.

[9] N. Fagnoni and E. de Lera Acedo. HERA Memo 21: An updated electromagnetic simulation of the HERA antenna with CST and comparison with measurements. *HERA Memo Series*, December 2016.